The Integrated Study on the Chemical Profiling to Explore the Constituents and Mechanism of Traditional Chinese Medicine Preparation Huatuo Jiuxin Pills Based on UPLC-Q-TOF/MS^E and Network Pharmacology

Yulong Zhu [1,2,3†], Yaqin Zhu [1,2,3†], Shuyue Tao [1,2,3], Wanhui Liang [1,2,3], Jing Zhang [1,2,3], Yunjing Zhang [1,2,3], Zihua Xuan [1], Jingjing Xu [1], Can Peng [1,2,3,4*], Huan Wu [1,2,3,4*] and Deling Wu [1,2,3,4*]

[1]School of Pharmacy, Anhui University of Chinese Medicine, Hefei, China, [2]Anhui Province Key Laboratory of Chinese Medicinal Formula, Hefei, China, [3]Anhui Province Key Laboratory of Pharmaceutical Preparation Technology and Application, Hefei, China, [4]Synergetic Innovation Center of Anhui Authentic Chinese Medicine Quality Improvement, Hefei, China

Huatuo Jiuxin Pills (HJP), a traditional Chinese medicine (TCM) preparation, has been widely used to treat Cardiovascular Diseases (CVDs) for more than 20 years. However, there were still gaps in the study of chemical components and potential pharmacological effects in the HJP. In this study, ultra-performance liquid chromatography-quadrupole time-of-flight mass spectrometry (UPLC-Q-TOF/MSE) combined with network pharmacology was used to comprehensively explore the chemical components in HJP and explore its potential active compounds and the mechanism for the treatment of CVDs. A total of 117 compounds, mainly including saponins, cholic acids, and bufadienolides, were rapidly identified and characterized. Simultaneously, the fragmentation mode and characteristic ion analysis of different types of representative compounds were carried out. Network pharmacology results showed that the more important active ingredients mainly include 5β-hydroxybufotalin, 19 oxo-cinobufagin, bufarenogin, etc. While, the main targets were PIK3CA, MAPK1, VEGFA and so on. Importantly, HJP has therapeutic effects on CVDs by acting on endocrine resistance, PI3K-Akt signaling pathway, HIF-1 signaling pathway, etc. In addition, molecular docking results showed that the core active ingredients with higher degrees in HJP have a strong affinity with the core targets of CVDs. The current work fills the gap in the chemical substance basis of HJP, and also facilitates a better understanding of the effective components, therapeutic targets, and signaling pathways of HJP in the treatment of CVDs.

Keywords: huatuo jiuxin pills, UPLC-Q-TOF/MSE, Cardiovascular Diseases, network pharmacology, molecular docking

1 INTRODUCTION

Cardiovascular Diseases (CVDs) were diseases with high morbidity and mortality (Taskinen and Borén, 2015; Halaris, 2017). Many risk factors may cause CVDs individually or in combination (Deprince et al., 2020). Currently, pharmaceutical chemicals are mainly used in clinical treatment with rapid and direct curative effects. They were usually used with other medicines, but long-term use was prone to adverse reactions (Damiani et al., 2020). Compared with chemical medications, traditional Chinese medicine (TCM) has the characteristics of multiple components, multiple targets, and fewer adverse effects (Wang et al., 2021a). So, it was more in line with the features of long-term medication for the treatment of CVDs. However, due to the complexity of components in TCM preparations, it is still a challenge to identify its effective ingredients, elucidate the mechanism, and discover the relationship between ingredients and therapeutic objectives (Luo et al., 2013).

Huatuo Jiuxin Pills (HJP), a classical TCM preparation, has been clinically used to treat CVDs in China for more than 20 years. It comprises eight crude TCM, i.e., *Panax ginseng C. A. Meyer* (Ren-Shen), *Panax notoginseng (Burk.) F. H. Chen* (San-Qi), *Venenum Bufonis* (Chan-Su), *Borneolum* (Bing-Pian), Artificial Calculus Bovis (Ren-Gong-Niu-Huang), Artificial Moschus (Ren-Gong-She-Xiang), Ox Bile Powder (Niu-Dan-Fen) and Pearl (Zhen-Zhu). The clinical study found that HJP has the function of promoting blood circulation, removing blood stasis, resolving phlegm and dredging collaterals (Zhou et al., 2020). In addition, Zhou's (Zhou et al., 2020) research also showed that HJP can significantly improve the blood stasis syndrome of experimental myocardial ischemia rats, and reduce its LDH and CPK levels in serum. However, the effective ingredients and *in vivo* action targets of HJP are still unknown, which limits the systematic understanding of the mechanism of HJP action.

In recent years, ultra-performance liquid chromatography-quadrupole time-of-flight mass spectrometry (UPLC-Q-TOF/MS^E) technology has provided a powerful method for efficient separation and structural characterization of TCM with high resolution, sensitivity, and accuracy (Xu et al., 2020). It is possible to obtain an accurate component precursor ion mass and fragment ions in the full scan mode, while increasing the reliability of the analysis results. And the UNIFI software was a multi-functional automatic data processing platform that can help process mass spectrometry data and quickly analyze chemical components. On the other hand, the mechanism of HJP in the treatment of CVDs and the key active compounds is still unclear. Faced with the current situation, we need an effective means to explore the relationship and mechanism between active components in HJP and core targets. The TCM network pharmacology method combined computational and experimental methods to analyze preparations and their action targets (Wang et al., 2021b), to understand the mechanism of action based on the biological molecular networks of diseases and syndromes. Furthermore, this method can also determine the network regulation mechanism and biological function of TCM, and discover new active compounds. It uncovers "drug-gene-disease" correlations, which are predictive and quantitative measures of the mechanism of action of TCM preparation in disease treatment (Li and Zhang, 2013).

The present study adopted the integration strategy of UPLC-Q-TOF/MS^E combined with the UNIFI platform to reveal the effective ingredients of HJP systematically. At the same time, network pharmacology and molecular docking were used to explore the active compounds of HJP and predict its potential targets and signal pathways for CVDs treatment. This study provides a certain basis and reference for the further study of the pharmacodynamic material basis and *in vivo* mechanism of HJP.

2 MATERIALS AND METHODS

2.1 Reagents and Materials

HJP was provided by Anhui Bozhou Huatuo National Pharmaceutical Co., Ltd. (Lot number: 20200601). Reference substances including ginsenoside Rd, pseudoginsenoside D, notoginsenoside R$_1$, ginsenoside Re, cinobufagin, bufalin, bufotalin, resibufogenin and cholic acid were all purchased from Chengdu Kromah Biotechnology Co., Ltd. Methanol and acetonitrile (MS grade) were purchased from Sigma-Aldrich (Shanghai) Trading Co., Ltd. Ultrapure water was obtained with the PALL laboratory water purification system (PALL, United States).

2.2 Standards and Sample Preparation

HJP was ground into powder and 0.3 g of powder was accurately weighed, dispersed in 30 ml methanol, extracted with ultrasonic (360 W, 40 kHz) in the water bath for 30 min. And then, it was filtrated through 0.22 μm filter membrane and the subsequent filtrate was transferred into autosampler vials for UPLC-Q-TOF/MS^E analysis. Nine reference standards (ginsenoside Rd, pseudoginsenoside D, notoginsenoside R$_1$, ginsenoside Re, cinobufagin, bufalin, bufotalin, resibufogenin and cholic acid) were dissolved in methanol and filtered through 0.22 μm filter membrane to prepare 1 mg/ml stock solution, respectively.

2.3 Chromatography and Mass Spectrometry Conditions

Chromatographic analysis was performed used Waters ACQUITY™ UPLC system (Waters Company, Milford, United States). Chromatographic separation was carried out at 30°C, using East Laboratory Epic C$_{18}$ column (100 mm × 2.1 mm, 1.8 μm) with mobile phases A (water) and B (acetonitrile).

The gradient profile was as follows: 0–4 min, 10–15% B; 4–5 min, 15–30% B; 5–11 min, 30% B; 11–15 min, 30–45% B; 15–21 min, 45–80% B; 21–29 min, 80–70% B; 29–30 min, 70–10% B. The flow rate was 0.2 ml/min, and the injection volume was 2 μL.

Mass spectrometric detection was performed on a Waters Xevo G2 Q-TOF mass spectrometer (Waters Corporation, Milford, United States) equipped with an ESI source. The full scan data was acquired from 50 to 1,200 Da, acquisition rate of 0.1 s, source temperature of 100°C, the source voltage of 3.2 kV. The collision voltage was set to 6.0 eV for low-energy scanning

and 20–60 eV for high-energy scanning. The nitrogen (N2) temperature was 300°C. In order to obtain the complete molecular fragmentation mode, the data-related collection was also carried out. And sample information was collected when the mass/charge ratio of correction solution leucine enkephalin (LE) was 556.2771 (positive ion mode) and 554.2615 (negative ion mode) to ensure the accuracy of the collected results.

2.4 Establishment of a Chemical Compound Library for HJP

The chemical composition system information of the eight Chinese medicines in HJP was collected and sorted through online database platforms such as China National Knowledge Infrastructure (CNKI[1]), Traditional Chinese Medicine Systems Pharmacology Database and Analysis Platform (TCMSP[2]), the Encyclopedia of Traditional Chinese Medicine (ETCM[3]), Chem Spider[4], and literature searches, etc. A self-built compound library containing compound name, molecular formula, chemical structure, and exact molecular weight was established by UNIFI software (**Supplementary Table S1**).

2.5 Data Analysis by UNIFI Platform

All MS data analysis was performed on the UNIFI software platform (Waters Corporation, Milford, United States). The acquisition time ranged from 1.5 min to 28.0 min. Quality inspection range: 50–1200 Da. The allowable range of quality error was within 5 ppm. The 2D peak intensity was set to a peak area greater than 100. The 3D peak intensity was greater than 200 for high-energy channels and greater than 300 for low-energy channels. The addition ions were +H, +Na (positive ion mode), and −H, +HCOO (negative ion mode). After all the data was analyzed and initially processed by the software, manual inspection and rechecking were still needed to investigate the chemical composition cracking pattern and enhance the accuracy of the characterization data.

2.6 Target Network Analysis

The targets were retrieved from the prediction of the online target platform Swiss Target Prediction[5]. "*Homo sapiens*" was the restrictor for target prediction. And the targets with a probability of more than 0.1 were collected. Meanwhile, the CVDs-related targets were obtained from the Gene cards database[6]. The Online Venn figure platform[7] was used to get the Venn figure and HJP with CVDs intersection of targets. Cytoscape software (version 3.2.1) was applied to construct the chemical-target and protein-protein interactions (PPIs) networks. All proteins/genes were subjected to pathway enrichment analysis (GO and KEGG analysis) using the

Metascape databases[8]. Those pathway terms with a *p*-value less than 0.05 were regarded as significant.

2.7 Molecular Docking

Download the protein PDB file of the core target from the RSCB PDB online platform[9] and the MOL2 file of the core active ingredient from PubChem database[10]. Auto Dock Tools (1.5.6, The Scripps Research Institute) software was used for molecular docking, and the docking results were imported into Pymol (2.5.0, Schrodinger, Inc.) software for visualization. Finally, the binding strength and activity of the active ingredients and the target were evaluated according to the binding energy.

3 RESULTS AND DISCUSSION

3.1 Identification and Characterization of Chemical Compounds

The high-resolution MS data of HJP were obtained by UPLC-Q-TOF/MS^E. The total ion chromatography (TIC) of HJP in positive and negative ion modes is shown in **Figure 1**. The UNIFI screening platform was used to analyze the collected MS^E data, and the mass error and responsivity were investigated by automatically matching ion fragments. After standard comparison, literature review and further manual verification, a total of 117 compounds in HJP were identified or tentatively characterized. They were classified by ingredient sources, including 32 triterpenoid saponins, 13 bile acids, 22 bufadienolides, etc. Then, the detailed MS information of these components was summarized in **Table 1**. In addition, we tentative confirmed the structures of these compounds based on accurate mass, MS^E data, and related literature. The compounds with the same core structure were classified, such as dammarane type and oleanane type. Finally, the structure of the main chemical components in HJP is shown in **Figure 2**.

3.2 Analysis of Chemical Component in HJP by UPLC/Q-TOF-MS^E

3.2.1 Triterpenoid Saponins

32 triterpenoid saponins were detected from HJP and were also the major bioactive constituents of *Panax ginseng C. A. Meyer* and *Panax notoginseng (Burk.) F. H. Chen*. These components have pharmacological effects such as cardiotonic, anti-oxidative stress, anti-myocardial ischemia, and immuno-enhancing function (Hu et al., 2018; Chen et al., 2020). The structure can also be divided into panaxadiol, panaxatriol, and oleanolic acid types. The primary fragmentation pattern of triterpenoid saponins was successive or simultaneous loss of the glycosidic unit at the site of C-20, C-3 or C-6 of ginsenosides until the formation of [Aglycon−H]$^-$ ions. MS data analysis revealed the

---

[8]https://metascape.org/gp/index.html#/main/step1.
[9]https://www1.rcsb.org/.
[10]https://pubchem.ncbi.nlm.nih.gov/.

FIGURE 1 | The TIC chromatograms of HJP from UPLC/Q-TOF-MS^E analysis.
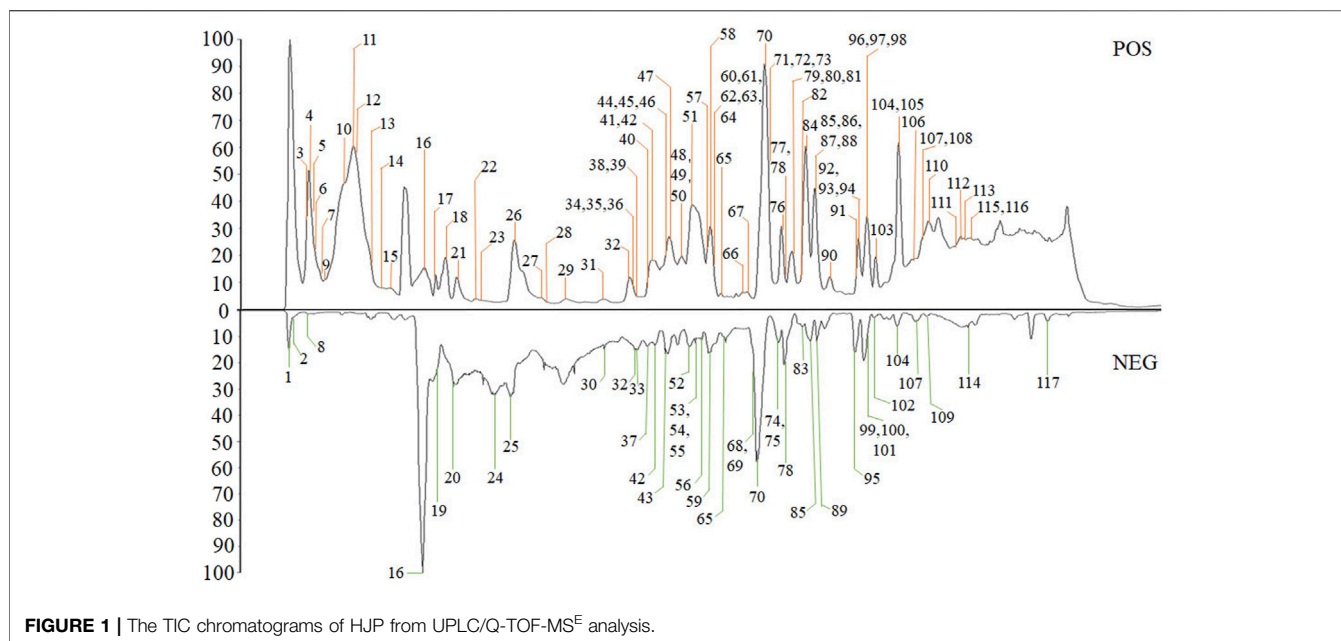
types and amount of glycosyl groups. For example, the mass differences of 162, 146 and 132Da suggested the presence of glucose (Glc), rhamnose (Rha), and xylose (Xyl), respectively (Fu et al., 2019).

Peak 16, peak 43, and peak 56 were identified as notoginsenoside R$_1$, pseudoginsenoside D, and ginsenoside Rd by comparing retention time and fragmentation patterns with reference standards. We investigated the MS fragmentation pattern of notoginsenoside R$_1$ in detail to facilitate the characterization of these ginsenosides (**Figure 3**). Notoginsenoside R$_1$ revealed quasi-molecular ion [M−H]$^-$ and [M + HCOO]$^-$ at m/z 931.5327 and 977.5309 in negative ion mode. And then [M−H]$^-$ ion lost a group of Xyl residue to form [M−H−Xyl]$^-$ ion at m/z 799.4813. The following succession to lose Glc residue to form m/z 637.4291 [M−H−Xyl−Glc]$^-$ and m/z 475.3743 [M−H−Xyl−2Glc]$^-$ ions. Hence, it was tentatively characterized as notoginsenoside R$_1$. In addition, the UNIFI software automatically matched the database with the acquisition mass spectrum data, and the compound was analyzed. Peak 36 had [M + H]$^+$ and [M + Na]$^+$ ions at m/z 801.4996 and 823.4800 in positive ion mode. The fragment ions of m/z 603.42470 and 585.4120 were formed under high collision energy. The mass error was within 0.10 ppm. The result of UNIFI platform matching for peak 36 was ginsenoside Rf. Through manual inspection and investigation of chemical structure, it is speculated that [M + H]$^+$ ion loses two H$_2$O and Glc residues, forming [M + H−2H$_2$O−Glc]$^+$ ion of m/z 603.4247. And then, it continued to lose the neutrality of H$_2$O, which formed [M + H−3H$_2$O−Glc]$^+$ ion of m/z 585.4120. Therefore, the compound was identified as ginsenoside Rf, and its chemical structural formula was C$_{42}$H$_{72}$O$_{14}$. Similarly, the matching result of compound 53 by UNIFI and manual verification shows ginsenoside Rg$_2$.

3.2.2 Cholic Acids

A total of 13 cholic acids were identified, which came from artificial *Calculus Bovis* and ox bile powder. These compounds have antipyretic, analgesic, cholagogic, anti-inflammatory, and detoxification effects (Xu et al., 2018; Floreani, 2020). They had a steroid parent nucleus in their structure and a pentanoic acid side chain at C-17. Due to the presence of polyhydroxy substituents and carboxyl groups in cholic acids, H$_2$O was often lost during the cleavage process to produce [M + H−H$_2$O]$^+$ or [M + H−2H$_2$O]$^+$. In addition to the above rules, a neutral loss of 75 and 125Da may occur in the cleavage pathway for the conjugated bile acid formed by the amide bond of glycine or taurine to free bile acid, indicating the loss of glycine (Gly) and taurine (Tau), respectively.

Peak 32 was unequivocally identified as taurocholic acid. The MS spectrum and possible fragmentation pattern of taurocholic acid were depicted in **Figure 4**. Taking taurocholic acid as an example, it produced fragment ions at m/z 516.2979 [M + H]$^+$, 480.2805 [M + H−2H$_2$O]$^+$, 462.2628 [M + H−3H$_2$O]$^+$, and 337.2517 [M + H−3H$_2$O−Tau]$^+$. Moreover, peak 73 had a protonated [M + H]$^+$ at m/z ion 431.2765 was identified as sodium cholate with a molecular formula of C$_{24}$H$_{39}$NaO$_5$, and formed characteristic ions at m/z 373.2751 [M + H−Na−2H$_2$O]$^+$ and m/z 254.2035 [M + H−Na−3H$_2$O−C$_5$H$_9$O$_2$]$^+$ through dehydration, sodium loss and C-17 valeric acid side chain dissociation. Their cleavage pathway conformed to the cleavage law of bile acids that were easy to lose H$_2$O. We also used UNIFI software to analyze the unknown compounds and performed manual testing on the matching results. For instance, peak 40 exhibited [M + H]$^+$ ion at m/z 488.2980, and UNIFI software speculated that its chemical formula was

TABLE 1 | Identification of chemical constituents of HJP by UPLC/Q–TOF–MS[E].

No	Formular	$t_{R(min)}$	Experimental mass (m/z)	Error (ppm)	MS and MS[E] data (+ or −) (m/z)	Compound identification	Source
1	$C_3H_7NO_2$	1.68	134.0456	−2.0	134.0456 [M + HCOO]⁻	Alanine	e, g, h
2	$C_7H_6O_3$	1.86	137.024	−3.4	137.024 [M−H]⁻ 93.0343 [M−H−COO]⁻	Salicylic acid	a
3	$C_{12}H_{22}O_{11}$	2.02	365.1047	−1.9	365.1047 [M + H]⁺ 165.0777 [M + H−Glc−O]⁺	Sucrose	a, b
4	$C_6H_{14}N_4O_2$	2.09	175.1193	2.3	175.1193 [M + H]⁺	Arginine	a, b, e, g, h
5	$C_{17}H_{26}O_2$	2.37	263.1996	−3.5	263.1996 [M + H]⁺ 156.1021 [M + H−2H₂O−C₅H₁₁]⁺	Ginsenoyne I	a
6	$C_8H_8O_2$	2.44	137.0603	4.2	137.0603 [M + H]⁺ 119.051 [M + H−H₂O]⁺ 77.0391 [M + H−H₂O−CH₃CO]⁺	Piceol	b
7	$C_9H_{11}NO_2$	2.51	180.1015	−2.1	180.1015 [M + H]⁺ 103.0548 [M−Ben]⁺ 91.0549 [M−C₃H₆NO₂]⁺ 77.0391 [Ben]⁺	Phenylalanine	e, g, h
8	$C_{10}H_{12}O_3$	2.85	225.0775	3.0	225.0775 [M + HCOO]⁻	3,5-Dimethoxyacetophenone	b
9	$C_{19}H_{26}O_3$	2.91	325.1763	−3.4	325.1763 [M + Na]⁺ 286.1576 [M + H−H₂O]⁺ 195.1141 [M + H−H₂O−CH₂CO−CH₂CH₃−O]⁺	Acetylpanaxydol	a
10	$C_{12}H_{16}N_2O$	3.3	205.1332	−1.7	205.1332 [M + H]⁺ 146.0607 [M + H−C₃H₉N]⁺	Bufotenine	c
11	$C_{17}H_{23}ClO_2$	3.84	317.1271	−2.6	317.1271 [M + Na]⁺ 89.0394 [M + H−2H₂O−C₁₀H₁₅Cl]⁺	Ginsenoyne B	a
12	$C_{13}H_{18}N_2O$	3.9	219.1491	−0.2	219.1491 [M + H]⁺ 160.0758 [M + H−C₃H₉N]⁺	Bufotenidine	c
13	$C_{27}H_{46}O_2$	4.26	425.3391	0.3	425.3391 [M + Na]⁺ 407.3308 [M + H−H₂O]⁺	7β-Hydroxycholesterol	c
14	$C_{36}H_{60}O_9$	4.36	637.4295	−2.4	637.4295 [M + H]⁺ 619.4187 [M + H−H₂O]⁺ 421.3459 [M + H−3H₂O−Glc]⁺	Ginsenoside Rh₇	a
15	$C_{12}H_{14}N_2O$	4.65	203.118	0.4	203.1181 [M + H]⁺ 87.0866 [M−CH₃]⁺	Dehydrobufotenine	c
16	$C_{47}H_{80}O_{18}$	6.35	977.5309	−1.8	977.5309 [M + HCOO]⁻ 799.4813 [M−H−Xyl]⁻ 637.4291 [M−H−Xyl−Glc]⁻ 475.3743 [M−H−Xyl−2Glc]⁻ 161.0429 [Glc−H]⁻	*Notoginsenoside R₁	b
17	$C_{26}H_{36}O_7$	6.58	461.2534	0	461.2534 [M + H]⁺ 275.1335 [M + H−2H₂O−α-pyr−CH₂COO]⁺	5β-Hydroxybufotalin	c
18	$C_{24}H_{32}O_6$	6.74	417.2281	2.3	417.2281 [M + H]⁺ 399.2173 [M + H−H₂O]⁺	Desacetylcinobufaginol	c
19	$C_{48}H_{82}O_{18}$	6.75	991.5471	−1.2	991.5471 [M + HCOO]⁻ 783.486 [M−H−Rha−O]⁻ 619.4148 [M−H−Rha−Glc−O]⁻	*Ginsenoside Re	a
20	$C_{42}H_{72}O_{14}$	6.88	845.4891	−1.5	799.4821 [M−H]⁻ 637.4300 [M−H−Rha−O]⁻ 475.3755 [M−H−Rha−Glc−O]⁻	Pseudoginsenoside F₁₁	a
21	$C_{15}H_{22}$	6.92	203.1797	1.4	203.1797 [M + H]⁺ 187.1485 [M−CH₃]⁺ 95.0865 [M−CH₃−C₇H₈]⁺	Cuparene	b
22	$C_{54}H_{92}O_{23}$	7.96	1,125.6079	2.5	1,125.6079 [M + H]⁺ 801.4995 [M + H−2Glc]⁺	Ginsenoside Rb₁	a
23	$C_{24}H_{34}O_6$	8.3	419.2421	−1.7	419.2421 [M + H]⁺ 347.2019 [M + H−4H₂O]⁺ 353.2111 [M + H−2H₂O−CH₂OH]⁺	Tetrahydroxybufa-20	c
24	$C_{41}H_{68}O_{14}$	8.98	829.456	−3.7	829.456 [M + HCOO]⁻ 499.2927 [M−H−2H₂O−Rha−C₅H₁₀O₂]⁻	Ginsenoside Rg₈	a
25	$C_{24}H_{32}O_6$	9.13	461.2176	−1.1	461.2176 [M + HCOO]⁻ 415.2116 [M−H]⁻	Psi-bufarenogin	c

(Continued on following page)

TABLE 1 | (Continued) Identification of chemical constituents of HJP by UPLC/Q–TOF–MS^E.

No	Formular	$t_{R(min)}$	Experimental mass (m/z)	Error (ppm)	MS and MS^E data (+ or –) (m/z)	Compound identification	Source
26	$C_{24}H_{32}O_6$	9.23	417.2275	0.9	397.1994 [M–H–H$_2$O]$^-$ 379.1873 [M–H–2H$_2$O]$^-$ 287.1641 [M–H–H$_2$O–α-pyr–CH$_3$]$^-$ 417.2275 [M + H]$^+$ 439.2096 [M + Na]$^+$ 399.2173 [M + H–H$_2$O]$^+$ 371.2211 [M + H–H$_2$O–CO]$^+$	Bufotalidin	c
27	$C_{41}H_{68}O_{13}$	10.13	783.4872	–2.1	783.4872 [M + H]$^+$ 441.3720 [M + H–H$_2$O–2Glc]$^+$ 423.3610 [M + H–2H$_2$O–2Glc]$^+$	Ginsenoside La	a
28	$C_{30}H_{48}O_3$	10.69	457.3666	–2.3	457.3666 [M + H]$^+$ 439.3586 [M + H–H$_2$O]$^+$ 421.3483 [M + H–2H$_2$O]$^+$	16-Oxoseratenediol	a
29	$C_9H_{10}O_3$	11.03	167.0708	3.5	167.0708 [M + H]$^+$ 93.0347 [M + H–CH$_3$CO–CH$_3$O]$^+$	Paeonol	a
30	$C_6H_{12}O_6$	12.06	534.1936	–0.8	534.1936 [M + HCOO]$^-$ 397.1625 [M–H–C$_2$H$_5$NO$_3$]$^-$	Galactose	a, h
31	$C_{24}H_{32}O_6$	12.21	473.2178	1.7	473.2178 [M + H]$^+$ 377.1715 [M + H–α-pyr]$^+$ 359.1651 [M + H–H$_2$O–α-pyr]$^+$	Bufarenogin	c
32	$C_{26}H_{45}NO_7S$	12.88	516.2979	–2	516.2979 [M + H]$^+$ 480.2805 [M + H–2H$_2$O]$^+$ 462.2668 [M + H–3H$_2$O]$^+$ 337.2517 [M + H–3H$_2$O–Tau]$^+$ 126.0220 [Tau]$^+$	Taurocholic acid	g
33	$C_{42}H_{72}O_{14}$	12.97	845.4927	2.7	845.4927 [M + HCOO]$^-$ 799.4867 [M–H]$^-$ 783.4883 [M–H–H$_2$O]$^-$ 637.4105 [M–H–Glc]$^-$ 161.0436 [Glc]$^-$	Ginsenoside Rg$_1$	a
34	$C_{24}H_{30}O_6$	13.11	415.212	1.2	457.3679 [M + H]$^+$ 397.1994 [M + H–H$_2$O]$^+$ 301.2499 [M + H–H$_2$O–α-pyr]$^+$	19-Oxodesacetylcinobufagin	c
35	$C_{30}H_{48}O_3$	13.15	457.3679	0.6	457.3679 [M + H]$^+$ 439.3573 [M + H–H$_2$O]$^+$ 421.3467 [M + H–2H$_2$O]$^+$	Oleanolic acid	a, b
36	$C_{42}H_{72}O_{14}$	13.19	801.4996	0.1	823.4800 [M + Na]$^+$ 801.4996 [M + H]$^+$ 603.42470 [M + H–2H$_2$O–Glc]$^+$ 585.4120 [M + H–3H$_2$O–Glc]$^+$	Ginsenoside Rf	a, b
37	$C_{26}H_{43}NO_6$	13.34	478.3153	–4.4	478.3153 [M + HCOO]$^-$ 327.2627 [M–H–gly–2CH$_3$]$^-$ 311.2639 [M–H–gly–2CH$_3$–O]$^-$	Glycocholic acid	e, g
38	$C_{24}H_{32}O_5$	13.41	401.2326	1	401.2326 [M + H]$^+$ 383.2170 [M + H–H$_2$O]$^+$ 365.2065 [M + H–2H$_2$O]$^+$ 347.1996 [M + H–3H$_2$O]$^+$	Resibufaginol	c
39	$C_{36}H_{62}O_{10}$	13.50	655.4413	–0.4	655.4413 [M + H]$^+$ 603.4237 [M + H–2H$_2$O–O]$^+$ 585.4097 [M + H–3H$_2$O–O]$^+$	Pseudoginsenoside RT$_5$	a
40	$C_{26}H_{42}NNaO_6$	13.83	488.298	–0.6	488.2980 [M + H]$^+$ 337.253 [M + H–Na–3H$_2$O–Gly]$^+$	Sodium glycocholate	e, g
41	$C_{48}H_{76}O_{19}$	13.86	979.4856	–1.7	979.4856 [M + Na]$^+$ 603.4229 [M + H–Glc–Glc-acid–H$_2$O]$^+$	Ginsenoside Ro	a, b
42	$C_{48}H_{82}O_{19}$	13.89	985.5356	1.4	985.5356 [M + Na]$^+$ 766.4859 [M + H–Glc–H$_2$O–O]$^+$	20-Glucoginsenoside Rf	a
43	$C_{54}H_{92}O_{23}$	14.16	1,107.5976	1.8	1,107.5976 [M–H]$^-$ 1,153.6048 [M + HCOO]$^-$ 945.5370 [M–H–Glc]$^-$ 783.4867 [M–H–2Glc]$^-$ 621.4408 [M–H–3Glc]$^-$	*Pseudoginsenoside D	a
44	$C_{41}H_{70}O_{13}$	14.2	771.4877	–1.5	771.4877 [M + H]$^+$ 605.4386 [M + H–H$_2$O–Xyl–O]$^+$	Notoginsenoside R$_2$	a

TABLE 1 | (*Continued*) Identification of chemical constituents of HJP by UPLC/Q–TOF–MS^E.

No	Formular	$t_{R(min)}$	Experimental mass (m/z)	Error (ppm)	MS and MS^E data (+ or −) (m/z)	Compound identification	Source
45	$C_{42}H_{72}O_{13}$	14.23	785.5029	−2.1	441.3715 [M + H–2H_2O–Xyl–Glc]$^+$ 425.3778 [M + H–2H_2O–Xyl–Glc–O]$^+$ 785.5029 [M + H]$^+$ 605.4386 [M + H–H_2O–Glc]$^+$ 459.3815 [M + H–2Glc]$^+$ 325.1133 [2Glc]$^+$	Ginsenoside Rg$_3$	a, b
46	$C_{24}H_{34}O_5$	14.44	403.2428	0.6	403.2428 [M + H]$^+$ 349.2166 [M + H–3H_2O]$^+$	1β-Hydroxybufalin	c
47	$C_{41}H_{68}O_{12}$	14.5	753.4775	−1.1	753.4775 [M + H]$^+$ 573.4102 [M + H–H_2O–Glc]$^+$	Ginsenoside Rg$_5$	a
48	$C_{24}H_{32}O_5$	14.83	401.2325	0.7	401.2325 [M + H]$^+$ 365.2127 [M + H–2H_2O]$^+$ 347.2006 [M + H–3H_2O]$^+$	Desacetylcinobufagin	c
49	$C_{36}H_{60}O_8$	14.94	621.4366	0.8	621.4366 [M + H]$^+$ 603.4243 [M + H–H_2O]$^+$ 441.372 [M + H–H_2O–Glc]$^+$	Ginsenoside Rh$_4$	a
50	$C_{53}H_{90}O_{22}$	14.95	1,079.5986	−1.0	1,079.5986 [M + H]$^+$ 1,104.7550 [M + Na]$^+$ 929.54 [M + H–H_2O–Fur]$^+$	Ginsenoside Rc	a, b
51	$C_{26}H_{36}O_6$	15.17	445.2588	0.6	445.2588 [M + H]$^+$ 467.2393 [M + Na]$^+$ 409.2319 [M + H–2H_2O]$^+$ 385.2365 [M + H–H_2O–CH_2CO]$^+$ 367.2268 [M + H–2H_2O–CH_2CO]$^+$ 349.2162 [M + H–α-pyr]$^+$ 331.1999 [M + H–H_2O–α-pyr]$^+$ 271.2065 [M + H–2H_2O–CH_2CO–α-pyr]$^+$	*Bufotalin	c
52	$C_{56}H_{94}O_{24}$	15.21	1,195.6054	−4.4	1,195.6054 [M + HCOO]$^−$ 1,149.6032 [M–H]$^−$ 943.5289 [M–H–CH_3CO–Glc]$^−$ 781.4687 [M–H–CH_3CO–2Glc]$^−$	Quinquenoside R$_1$	a
53	$C_{42}H_{72}O_{13}$	15.23	807.485	−1.9	807.4850 [M + Na]$^+$ 621.4353 [M + H–H_2O–Rha]$^+$ 423.36173 [M + H–3H_2O–Rha–Glc]$^+$	Ginsenoside Rg$_2$	a
54	$C_{36}H_{54}O_{10}$	15.26	647.3804	2.1	647.3804 [M + H]$^+$ 385.2364 [M + H–GlcUA–C_6H_{12}]$^+$ 367.2268 [M + H–H_2O–GlcUA–C_6H_{12}]$^+$	Gypsogenin-3-glucoronide	a
55	$C_{26}H_{32}O_7$	15.41	457.2223	0.5	457.2223 [M + H]$^+$ 439.3511 [M + H–H_2O]$^+$ 332.1877 [M + H–α-pyr–CHO]$^+$	19-Oxocinobufagin	c
56	$C_{48}H_{82}O_{19}$	15.64	991.5519	3.6	991.5519 [M + HCOO]$^−$ 783.4906 [M–H–Glc]$^−$ 621.4358 [M–H–2Glc]$^−$	*Ginsenoside Rd	a, b
57	$C_{42}H_{70}O_{12}$	15.68	767.4924	−2.1	767.4924 [M + H]$^+$ 605.4392 [M + H–Rha–O]$^+$ 443.3875 [M + H–Rha–Glc–O]$^+$	Ginsenoside Rg$_4$	a
58	$C_{18}H_{32}O_{16}$	15.71	505.1781	3.5	505.1781 [M + H]$^+$ 487.1651 [M + H–H_2O]$^+$ 325.1127 [M + H–H_2O–Glc]$^+$ 163.0503 [M + H–H_2O–2Glc]$^+$	Panose	a
59	$C_{36}H_{62}O_9$	15.76	683.4398	3.2	683.4398 [M + HCOO]$^−$ 637.4327 [M–H]$^−$ 475.3783 [M–H–Glc]$^−$ 391.2803 [M–H–Glc–C_6H_{12}]$^−$ 161.0439 [Glc]$^−$	Ginsenoside Rh$_1$	a
60	$C_{26}H_{34}O_7$	15.79	459.2373	−0.9	459.2373 [M + H]$^+$ 381.2055 [M + H–H_2O–α-pyr]$^+$ 363.1952 [M + H–α-pyr]$^+$	Cinobufaginol	c
61	$C_{14}H_{24}O$	15.81	231.1718	−0.8	231.1718 [M + Na]$^+$ 213.1633 [M + H–H_2O]$^+$ 147.1169 [M + H–H_2O–C_3H_7]$^+$	1-Ethynylcyclododecanol	f
62	$C_{36}H_{62}O_9$	15.82	639.4436	−4.8	661.4256 [M + Na]$^+$	Ginsenoside F$_1$	a

TABLE 1 | (*Continued*) Identification of chemical constituents of HJP by UPLC/Q–TOF–MS^E.

No	Formular	$t_{R(min)}$	Experimental mass (m/z)	Error (ppm)	MS and MS^E data (+ or –) (m/z)	Compound identification	Source
					639.4436 [M + H]$^+$		
					459.3836 [M + H–Glc–H$_2$O]$^+$		
					423.3620 [M + H–3H$_2$O–Glc]$^+$		
					405.3513 [M + H–4H$_2$0–Glc]$^+$		
63	C$_{15}$H$_{24}$O	15.85	221.1896	–1.6	221.1896 [M + H]$^+$	Spathulenol	a, b
					203.1793 [M + H–H$_2$O]$^+$		
					187.1480 [M–H$_2$O–CH$_3$]$^+$		
64	C$_{28}$H$_{48}$O	15.91	423.3617	4.6	423.3617 [M + Na]$^+$	Campesterol	a
					383.2178 [M + H–H$_2$O]$^+$		
					311.2708 [M–H$_2$O–C$_5$H$_{11}$]$^+$		
65	C$_{26}$H$_{44}$NNaO$_6$S	16.31	522.2867	1.5	522.2867 [M + H]$^+$	Taurohyodeoxycholic acid sodium salt	e
					339.2702 [M + H–Na–2H$_2$O–Tau]$^+$		
66	C$_{47}$H$_{80}$O$_{17}$	17.06	917.5485	1.8	939.5303 [M + Na]$^+$	Gypenoside ix	b
					917.5485 [M + H]$^+$		
					719.4701 [M + H–2H$_2$O–Glc]$^+$		
					587.4297 [M + H–2H$_2$O–Xyl–Glc]$^+$		
67	C$_{36}$H$_{62}$O$_8$	17.11	645.4357	3.1	645.4357 [M + Na]$^+$	20(S)-Protopanaxadiol saponins	a
					587.4297 [M + H–2H$_2$O]$^+$		
					425.3789 [M + H–2H$_2$O–Glc]$^+$		
					407.3684 [M + H–3H$_2$O–Glc]$^+$		
68	C$_{23}$H$_{38}$O$_2$	17.39	345.2795	–1.1	345.2795 [M–H]$^-$	5-Resorcinol	a
					205.1576 [M–H–C$_{10}$H$_{20}$]$^-$		
69	C$_{24}$H$_{40}$O$_5$	17.4	407.2798	–1.3	453.2850 [M + HCOO]$^-$	*Cholic acid	e, g
					407.2798 [M–H]$^-$		
					389.2656 [M–H–H$_2$O]$^-$		
					363.2880 [M–H–COO]$^-$		
70	C$_{24}$H$_{34}$O$_4$	17.49	387.2544	3.7	409.2367 [M + Na]$^+$	*Bufalin	c
					387.2544 [M + H]$^+$		
					369.2441 [M + H–H$_2$O]$^+$		
					351.2336 [M + H–2H$_2$O]$^+$		
					291.2113 [M + H–α-pyr]$^+$		
					255.2109 [M + H–2H$_2$O–α-pyr]$^+$		
71	C$_{17}$H$_{22}$O$_2$	17.66	259.169	–1.0	259.1690 [M + H]$^+$	Ginsenoyne A	a
					227.1803 [M + H–2O]$^+$		
					199.1488 [M + H–2O–C$_2$H$_4$]$^+$		
72	C$_{15}$H$_{18}$	17.68	199.1488	3.2	199.1488 [M + H]$^+$	Cadalene	b
					184.1220 [M + H–CH$_3$]$^+$		
					169.1018 [M + H–2CH$_3$]$^+$		
73	C$_{24}$H$_{39}$NaO$_5$	17.71	431.2765	–0.6	431.2765 [M + H]$^+$	Sodium cholate	g
					373.2751 [M + H–Na–2H$_2$O]$^+$		
					355.2647 [M + H–Na–3H$_2$O]$^+$		
					337.2539 [M + H–Na–4H$_2$O]$^+$		
					254.2035 [M + H–Na–3H$_2$O–C$_5$H$_9$O$_2$]$^+$		
74	C$_{32}$H$_{46}$O$_8$	17.91	557.3112	–1.4	557.3112 [M–H]$^-$	Gamabufotalin-3-hydrogen suberate	c
					461.283 [M–H–α-pyr]$^-$		
					383.2164 [M–H–SA]$^-$		
					173.0804 [SA–H]$^-$		
75	C$_{26}$H$_{45}$NO$_6$S	17.96	500.3028	–2.5	500.3028 [M + H]$^+$	Tauroursodeoxycholic acid	e, g
					339.268 [M + H–2H$_2$O–Tau]$^+$		
76	C$_{26}$H$_{45}$NO$_6$	18	450.3213	–0.1	472.3027 [M + Na]$^+$	Glycodeoxycholic acid	e, g
					450.3213 [M + H]$^+$		
					339.2680 [M + H–2H$_2$O–Gly]$^+$		
					297.2643 [M + H–2H$_2$O–Gly–CH$_2$CO]$^+$		
77	C$_2$6H$_{42}$NNaO$_5$	18.21	472.3027	–1.3	472.3027 [M + H]$^+$	Sodium glycodeoxycholate	e
					339.2683 [M + H–Na–2H$_2$O–Gly]$^+$		
					297.2643 [M + H–Na–2H$_2$O–Gly–CH$_2$CO]$^+$		
78	C$_{36}$H$_{60}$O$_7$	18.48	605.4411	–0.2	621.4298 [M + Na]$^+$	Ginsenoside Rh$_3$	a
					605.4411 [M + H]$^+$		
					425.3780 [M + H–H$_2$O–Glc]$^+$		
					407.3673 [M + H–2H$_2$O–Glc]$^+$		
79	C$_{10}$H$_{16}$O	18.51	153.1277	2.3	153.1277 [M + H]$^+$	Isopulegone	b
					123.1168 [M + H–2CH$_3$]$^+$		

(Continued on following page)

TABLE 1 | (Continued) Identification of chemical constituents of HJP by UPLC/Q–TOF–MS^E.

No	Formular	$t_{R(min)}$	Experimental mass (m/z)	Error (ppm)	MS and MS^E data (+ or –) (m/z)	Compound identification	Source
80	$C_{19}H_{32}O_2$	18.58	315.2297	0.8	315.2297 [M + Na]$^+$ 257.2265 [M + H–2H$_2$O]$^+$	Dihydroandrosterone	f
81	$C_{30}H_{48}O_5$	18.61	489.3577	0.4	489.3577 [M + H]$^+$ 471.3469 [M + H–H$_2$O]$^+$ 453.3401 [M + H–2H$_2$O]$^+$ 435.3232 [M + H–3H$_2$O]$^+$	Asiatic acid	d
82	$C_{38}H_{58}N_4O_8$	18.82	699.4322	–0.7	699.4322 [M + H]$^+$ 681.4213 [M + H–H$_2$O]$^+$ 351.2333 [M + H–H$_2$O–Sub]$^+$	Bufalitoxin	c
83	$C_{24}H_{38}O_4$	18.94	389.2688	–2.3	435.2749 [M + HCOO]$^-$ 389.2688 [M–H]$^-$ 374.2522 [M–H–CH$_3$]$^-$ 332.2039 [M–H–C$_4$H$_9$]$^-$	Diisooctyl phthalate	a
84	$C_{26}H_{34}O_6$	19.02	443.2428	0	465.2243 [M + Na]$^+$ 443.2428 [M + H]$^+$ 347.2005 [M + H–α–pyr]$^+$ 425.2307 [M + H–H$_2$O]$^+$ 383.2217 [M + H–H$_2$O–CH$_2$CO]$^+$ 365.2111 [M + H–2H$_2$O–CH$_2$CO]$^+$ 337.2166 [M + H–2H$_2$O–CH$_2$CO–CO]$^+$ 319.2060 [M + H–3H$_2$O–CH$_2$CO–CO]$^+$	*Cinobufagin	c
85	$C_{24}H_{30}O_5$	19.26	399.2164	–0.5	399.2164 [M + H]$^+$ 267.2266 [M + H–2O]$^+$ 271.2057 [M + H–α–pyr–2O]$^+$	3-Hydroxy-19-oxo-14, 15-epoxybufa-20,22-dienolide	c
86	$C_{32}H_{44}O_9$	19.28	595.2865	–2.0	595.2865 [M + Na]$^+$ 399.2169 [M + H–SA]$^+$ 271.2057 [M + H–SA–α–pyr–2O]$^+$	Arenobufagin 3-hemisuberate	c
87	$C_{24}H_{32}O_4$	19.32	385.2372	–0.3	407.2186 [M + Na]$^+$ 385.2372 [M + H]$^+$ 253.1949 [M + H–2H$_2$O–α-pyr]$^+$	*Resibufogenin	c
88	$C_{10}H_{16}$	19.34	137.1327	1.8	137.1327 [M + H]$^+$ 121.1014 [M–CH$_3$]$^+$ 107.0861 [M + H–2CH$_3$]$^+$	Beta-pinene	b
89	$C_{30}H_{50}O_2$	19.55	443.3869	3.2	443.3869 [M + H]$^+$ 425.3776 [M + H–H$_2$O]$^+$ 407.3664 [M + H–2H$_2$O]$^+$	Erythrodiol	d
90	$C_{19}H_{34}O_2$	19.62	317.2438	–4	317.2438 [M + Na]$^+$ 137.1325 [M + H–C$_9$H$_{18}$O$_2$]$^+$	Methyl linoleate	a
91	$C_{24}H_{39}NaO_4$	20.67	415.2822	0.8	415.2822 [M + H]$^+$ 339.2690 [M + H–2H$_2$O–Na–OH]$^+$	Sodium deoxycholate	g
92	$C_{19}H_{30}O_2$	20.74	313.2139	0.2	313.2139 [M + Na]$^+$ 275.2003 [M–CH$_3$]$^+$ 257.1884 [M–H$_2$O–CH$_3$]$^+$	Etiocholanolone	f
93	$C_{38}H_{56}O_4$	20.79	599.4081	1.7	599.40813 [M + Na]$^+$ 81.2788 [M + H–Ferulic-acid]$^+$	Campesteryl ferulate	a
94	$C_{24}H_{40}O_4$	20.85	393.3006	1.7	393.3006 [M + H]$^+$ 375.2897 [M + H–H$_2$O]$^+$ 357.2793 [M + H–2H$_2$O]$^+$ 275.2003 [M + H–H$_2$O–C$_5$H$_9$O–CH$_3$]$^+$	Murocholic acid	e
95	$C_{24}H_{40}O_4$	20.98	391.2849	–1.2	391.2849 [M–H]$^-$ 373.2694 [M–H–H$_2$O]$^-$ 355.2620 [M–H–2H$_2$O]$^-$	Deoxycholic acid	e, g
96	$C_{16}H_{28}O$	21.02	237.2217	1.6	237.2217 [M + H]$^+$ 81.0707 [M + H–C$_{10}$H$_{19}$O]$^+$	(1S,15S)-bicyclohexadecan	f
97	$C_{15}H_{24}$	21.05	227.1776	2.4	227.1776 [M + Na]$^+$ 161.1329 [M + H–C$_3$H$_8$]$^+$	α-Muurolene	a, b
98	$C_{30}H_{50}O_3$	21.06	459.3841	1.7	459.3841 [M + H]$^+$ 441.3733 [M + H–H$_2$O]$^+$ 423.3628 [M + H–2H$_2$O]$^+$ 339.2693 [M + H–H$_2$O–C$_6$H$_{12}$]$^+$	Dryobalanone	d
99	$C_{15}H_{22}$	21.08	203.1794	–0.2	203.1794 [M + H]$^+$ 161.1329 [M + H–C$_3$H$_6$]$^+$ 147.1174 [M + H–C$_4$H$_8$]$^+$	α-Curcumene	a

(Continued on following page)

TABLE 1 | (*Continued*) Identification of chemical constituents of HJP by UPLC/Q–TOF–MS^E.

No	Formular	$t_{R(min)}$	Experimental mass (m/z)	Error (ppm)	MS and MS^E data (+ or –) (m/z)	Compound identification	Source
100	$C_{30}H_{52}O_4$	21.11	477.3951	2.7	477.3951 [M + H]$^+$ 459.3841 [M + H–H$_2$O]$^+$ 441.3733 [M + H–2H$_2$O]$^+$ 423.3628 [M + H–3H$_2$O]$^+$	Protopanaxatriol	a, b
101	$C_{20}H_{40}N_2O_8$	21.15	435.2772	–2.7	435.2772 [M–H]$^-$ 389.2665 [M–H–H$_2$O–CO]$^-$	6-O-Hexonic acid	a
102	$C_{53}H_{92}O_7$	21.36	841.6895	–2.4	841.6895 [M + H]$^+$ 703.5716 [M + H–3H$_2$O–C$_6$H$_{12}$]$^+$	Sitoindoside II	a
103	$C_{30}H_{50}O_2$	22.20	443.3904	4.7	443.3904 [M + H]$^+$ 425.3778 [M + H–H$_2$O]$^+$	Dipterocarpol	d
104	$C_{12}H_{25}NO$	22.38	200.2004	–2.5	200.2004 [M + H]$^+$ 184.1692 [M–CH$_3$]$^+$	Dimethyldecanamide	a
105	$C_{15}H_{26}O_2$	22.42	239.2	–2.2	239.2002 [M + H]$^+$ 221.2264 [M + H–H$_2$O]$^+$	4,10-Aromadendranediol	a
106	$C_{18}H_{30}O_2$	22.78	279.2325	2.3	279.2325 [M + H] $^+$ 261.2206 [M + H–H$_2$O]$^+$ 95.0863 [M + H–H$_2$O–CH$_2$CO–C$_9$H$_{16}$]$^+$	Linolenic acid	a
107	$C_{20}H_{38}O_2$	22.86	311.2948	1.1	311.2948 [M + H]$^+$ 250.1584 [M + H–H$_2$O–CH2CO]$^+$	Eicosenoic acid	a
108	$C_{34}H_{46}O_9$	22.90	599.3223	1.5	621.3052 [M + Na]$^+$ 599.3223 [M + H]$^+$ 425.2326 [M + H–SA]$^+$	Cinobufagin-3-hydrogen suberate	c
109	$C_{42}H_{82}NO_{10}P$	23.01	790.5596	–1.0	790.5596 [M–H]$^-$ 480.3076 [M–H–CO$_2$–C$_{18}$H$_{34}$O]$^-$	Phosphatidylserine	a
110	$C_{24}H_{50}NO_7P$	23.2	496.34	0.5	496.3400 [M + H]$^+$ 478.3293 [M + H–H$_2$O]$^+$ 313.2740 [M + H–C$_5$H$_{15}$NO$_4$P]$^+$ 184.0736 [M + H–C$_{19}$H$_{37}$O$_3$]$^+$	lysolecithin	g
111	$C_{16}H_{25}N$	24.08	232.2064	1.7	232.2064 [M + H]$^+$ 215.1766 [M–CH$_3$]$^+$	Muscopyridine	f
112	$C_{41}H_{84}N_2O_6P$	24.17	731.6041	–2.8	731.6041 [M + H]$^+$ 184.0732 [M + H–C$_{36}$H$_{69}$NO$_2$]$^+$	Sphingomyelin	g
113	$C_{30}H_{52}O_4$	24.34	499.3753	–1.0	499.3753 [M + Na]$^+$ 399.2156 [M + H–H$_2$O–2CH$_3$]$^+$	Panaxatriol	b
114	$C_{24}H_{40}O_3$	24.37	375.2894	–3.0	375.2894 [M–H]$^-$	Lithocholic acid	e, g
115	$C_{16}H_{30}O_2$	25.00	277.2143	1.7	277.2143 [M + Na]$^+$	13-Tetradecen acetate	a
116	$C_{20}H_{32}O_2$	25.54	305.2467	–2.7	305.2467 [M + H]$^+$ 289.2157 [M–CH$_3$]$^+$ 243.2094 [M + H–CH$_3$–HCOO]$^+$	Arachidonate	a
117	$C_{18}H_{32}O_2$	27.13	279.2318	–4.0	279.2318 [M–H]$^-$ 179.1058 [M–H–C$_7$H$_{16}$]$^-$ 163.1109 [M–H–C$_6$H$_{13}$–OCH$_3$]$^-$	Methyl heptadecadienoate	b

Glc: glucose; Rha: rhamnose; Xyl: xylose; Gly: glycine; GlcUA: glucuronic acid; α-pyr: α-pyrone; Sub: suberylarginine; SA: suberic acid; Tau: taurine.
[a]*Panax ginseng C. A. Meyer.*
[b]*Panax notoginseng (Burk.) F. H. Chen.*
[c]*Venenum Bufonis.*
[d]*Borneolum.*
[e]*Artificial Calculus Bovis.*
[f]*Artificial Moschus.*
[g]*Ox Bile Powder.*
[h]*Pearl.*
Identified by comparison with reference standards (Supplementary Figure S1**).*

$C_{26}H_{42}NNaO_6$. The manual analysis found it generated an [M + H–Na–3H$_2$O–Gly]$^+$ ion at *m/z* 337.2530 by the loss of Na$^+$, 3H$_2$O and Gly residue. Thus, peak 40 was assigned as sodium glycocholate. Similarly, through UNIFI platform matching, the preliminary results showed that the peak 95 is deoxycholic acid.

3.2.3 Bufadienolides

22 bufadienolides were identified in HJP, which were derived from *Venenum Bufonis*. It has a strong cardiac excitatory effect like that of digitalis. Importantly, the drug possessed many advantages such as quick-acting, no accumulation and diuretic action (Wansapura et al., 2009; Xie et al., 2016; Zhang et al.,
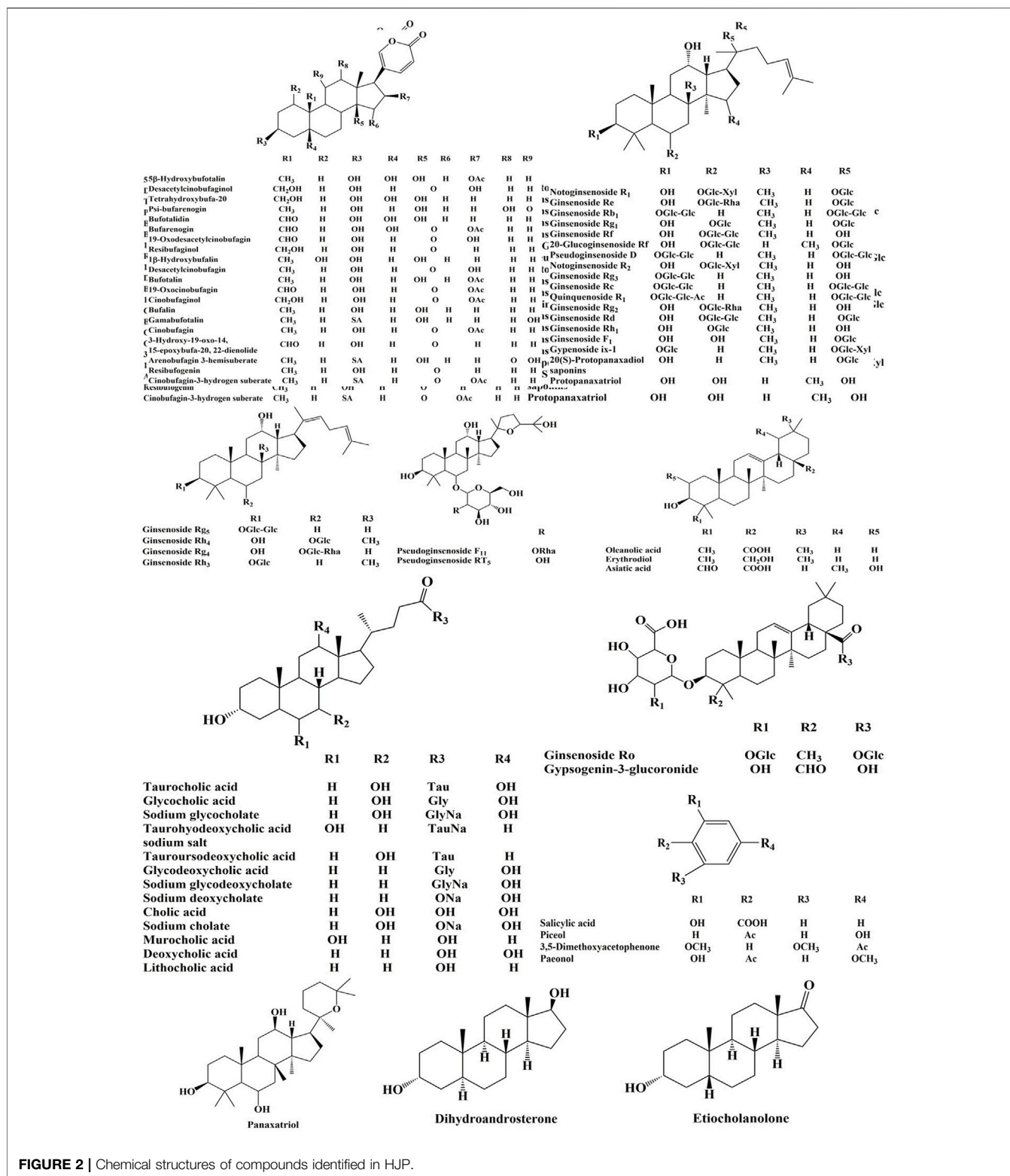
Bufadienolides (R1–R9)

	R1	R2	R3	R4	R5	R6	R7	R8	R9
5β-Hydroxybufotalin	CH3	H	OH	OH	OH	H	OAc	H	H
Desacetylcinobufaginol	CH2OH	H	OH	H	O		OH	H	H
Tetrahydroxybufa-20	CH2OH	H	OH	OH	OH	H	H	H	H
Psi-bufarenogin	CH3	H	OH	OH	OH	H	H	OH	O
Bufotalidin	CHO	H	OH	OH	OH	H	H	H	H
Bufarenogin	CHO	H	OH	OH	H	O	OAc	H	H
19-Oxodesacetylcinobufagin	CHO	H	OH	H	O		OH	H	H
Resibufaginol	CH2OH	H	OH	H	O		H	H	H
1β-Hydroxybufalin	CH3	OH	OH	H	OH	H	H	H	H
Desacetylcinobufagin	CH3	H	OH	H	O		H	H	H
Bufotalin	CH3	H	OH	H	OH	H	OAc	H	H
19-Oxocinobufagin	CHO	H	OH	H	O		OAc	H	H
Cinobufaginol	CH2OH	H	OH	H	O		OAc	H	H
Bufalin	CH3	H	OH	H	OH	H	H	H	H
Gamabufotalin	CH3	H	SA	H	OH	H	H	H	H
Cinobufagin	CH3	H	OH	H	O		OAc	H	H
3-Hydroxy-19-oxo-14,15-epoxybufa-20,22-dienolide	CHO	H	OH	H	O		H	H	H
Arenobufagin 3-hemisuberate	CH3	H	SA	H	OH	H	H	H	O
Resibufogenin	CH3	H	OH	H	O		H	H	H
Cinobufagin-3-hydrogen suberate	CH3	H	SA	H	O		OAc	H	H

Ginsenosides (R1–R5)

	R1	R2	R3	R4	R5
Notoginsenoside R1	OH	OGlc-Xyl	CH3	H	OGlc
Ginsenoside Re	OH	OGlc-Rha	CH3	H	OGlc
Ginsenoside Rb1	OGlc-Glc	H	CH3	H	OGlc-Glc
Ginsenoside Rg1	OH	OGlc	CH3	H	OGlc
Ginsenoside Rf	OH	OGlc-Glc	CH3	H	OH
G20-Glucoginsenoside Rf	OH	OGlc-Glc	CH3	H	OGlc
Pseudoginsenoside D	OGlc-Glc	H	CH3	H	OGlc-Glc
Notoginsenoside R2	OH	OGlc-Xyl	CH3	H	OH
Ginsenoside Rg3	OGlc-Glc	H	CH3	H	OH
Ginsenoside Rc	OGlc-Glc	H	CH3	H	OGlc-Glc
Quinquenoside R1	OGlc-Glc-Ac	H	CH3	H	OGlc-Glc
Ginsenoside Rg2	OH	OGlc-Rha	CH3	H	OH
Ginsenoside Rd	OH	OGlc-Glc	CH3	H	OGlc
Ginsenoside Rh1	OH	OGlc	CH3	H	OH
Ginsenoside F1	OH	OH	CH3	H	OGlc
Gypenoside ix-1	OGlc	H	CH3	H	OGlc
20(S)-Protopanaxadiol	OH	H	CH3	H	OGlc
Protopanaxatriol	OH	OH	H	CH3	OH

Ginsenoside Rg5 series (R1–R3)

	R1	R2	R3
Ginsenoside Rg5	OGlc-Glc	H	H
Ginsenoside Rh4	OH	OGlc	CH3
Ginsenoside Rg4	OH	OGlc-Rha	H
Ginsenoside Rh3	OGlc	H	CH3

	R
Pseudoginsenoside F11	ORha
Pseudoginsenoside RT5	OH

Oleanane type (R1–R5)

	R1	R2	R3	R4	R5
Oleanolic acid	CH3	COOH	CH3	H	H
Erythrodiol	CH3	CH2OH	CH3	H	H
Asiatic acid	CHO	COOH	H	CH3	OH

Bile acids (R1–R4)

	R1	R2	R3	R4
Taurocholic acid	H	OH	Tau	OH
Glycocholic acid	H	OH	Gly	OH
Sodium glycocholate	H	OH	GlyNa	OH
Taurohyodeoxycholic acid sodium salt	OH	H	TauNa	H
Tauroursodeoxycholic acid	H	OH	Tau	H
Glycodeoxycholic acid	H	H	Gly	OH
Sodium glycodeoxycholate	H	H	GlyNa	OH
Sodium deoxycholate	H	H	ONa	OH
Cholic acid	H	OH	OH	OH
Sodium cholate	H	OH	ONa	OH
Murocholic acid	OH	H	OH	OH
Deoxycholic acid	H	H	OH	OH
Lithocholic acid	H	H	OH	H

	R1	R2	R3
Ginsenoside Ro	OGlc	CH3	OGlc
Gypsogenin-3-glucoronide	OH	CHO	OH

Phenolics (R1–R4)

	R1	R2	R3	R4
Salicylic acid	OH	COOH	H	H
Piceol	H	Ac	H	OH
3,5-Dimethoxyacetophenone	OCH3	H	OCH3	Ac
Paeonol	OH	Ac	H	OCH3

Panaxatriol   Dihydroandrosterone   Etiocholanolone

FIGURE 2 | Chemical structures of compounds identified in HJP.

2019a). These components have a higher response in the positive ion mode, and there were [M + H]$^+$ quasi-molecular ions. Due to the polyhydroxy and α-pyrone (α-pyr) in its structure, it was easy to lose H$_2$O (18 Da) and α-pyr (96 Da) residue under high collision energy in mass spectrometry. In addition, deacetylation caused a neutral loss of 60 Da.

Peaks 51 was identified as bufotalin, which belongs to bufadienolides, based on retention time and fragment behavior

FIGURE 3 | The MS spectra and fragmentation pattern of notoginsenoside R_1 in negative ion mode.
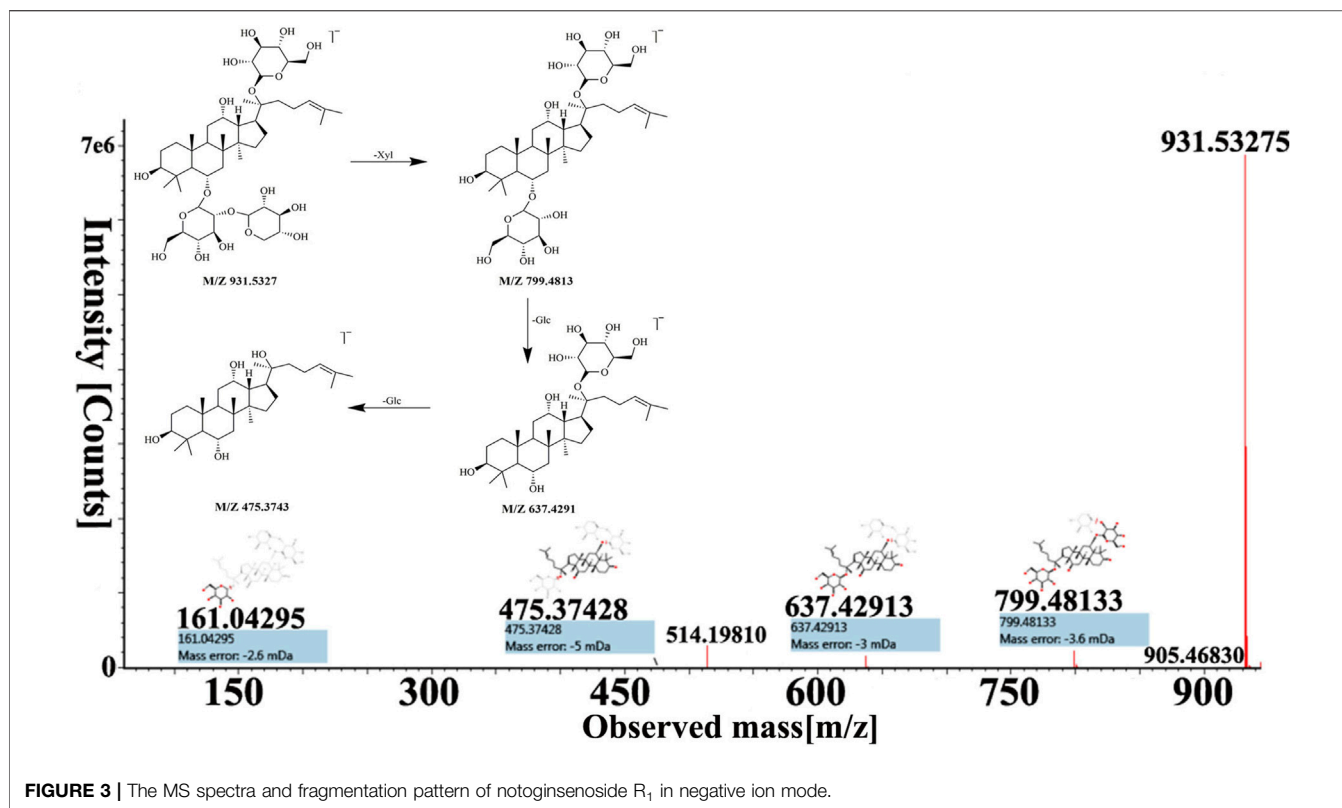
of reference standard. Bufotalin showed $[M + H]^+$ and $[M + Na]^+$ ions at m/z 445.2588 and 467.2393. Next, it underwent deacetylations and dehydrations to form $[M + H-H_2O-CH_2CO]^+$ and $[M + H-2H_2O-CH_2CO]^+$ fragment ions at m/z 385.2365 and 367.2268. And then, dissociation of the α-pyran ring gave rise to $[M + H-2H_2O-CH_2CO-\alpha\text{-pyr}]^+$ ion at m/z 271.2065. Furthermore, it directly lost the α-pyr and then lost H_2O to obtain fragment ions of m/z 349.2162 and 331.1999, respectively. The high-energy MS spectra and the proposed fragment pathway of bufotalin are depicted in **Figure 5**. Peaks 60, 70, 84, and 87 have similar cleavage rules of bufotalin, and all have the neutral loss of the characteristic fragment ions of the α-pyrone. By matching with UNIFI software and comparing with standard products, they were identified as cinobufaginol, bufalin, cinobufagin, and resibufogenin.

3.2.4 Others

In addition to the three major components, we also identified indole alkaloids (3), amino acids (4), organic acids (6), polysaccharides (3), lecithins (2), and volatile oils (23). These compounds showed higher responses in the positive ion mode, in the form of $[M + H]^+$ ions. And there were usually contains hydroxyl groups and other easy-to-lost groups in the structure of these components, which generated $[M + H-H_2O]^+$ or $[M + H-2H_2O]^+$ ions, etc. at high collision energies. Taking peaks 80 and 89 as examples, peak 80 showed $[M + H]^+$ and $[M + Na]^+$ ions at m/z 293.2557 and 315.2297. The mass error range was within 0.8 ppm. It continuously lost two H_2O under high collision

energy and obtained $[M + H-2H_2O]^+$ ion with m/z 257.2265, identified as dihydroandrosterone. Similarly, peak 89 has an $[M + H]^+$ ion of m/z 443.3869 in the positive ion mode. Then, by continuously losing H_2O $[M + H-H_2O]^+$ and $[M + H-2H_2O]^+$ fragment examples were formed at m/z 425.3776 and 407.3664, and the compound was finally identified as erythrodiol.

3.3 Network Pharmacology Research
3.3.1 Target Prediction and Screening

Generally speaking, molecules with oral bioavailability (OB) $\geq$ 30% and drug-like properties (DL) $\geq$ 0.18 are considered to have better pharmacological effects (Wei et al., 2020). We reference the OB and DL values combined with Swiss ADME (http://www.swissadme.ch/) to screen the ingredients with high gastrointestinal absorption, and a total of 26 active ingredients were obtained (**Table 2**). Then, the disease-related target proteins and gene targets were obtained through the Swiss Target Prediction, Gene Cards, Uniprot, and OMIM database. A total of 276 drug-related and 1,293 CVDs-related targets were obtained.

3.3.2 Construction of D-I-T and PPI Network

The drug-ingredient-target (D-I-T) network contains 308 nodes, including six drugs, 26 active compounds, and 276 targets (**Figure 6**). The ingredient that corresponded to more targets meant more importance. According to the degree analysis, the top three compounds were 5β-hydroxybufotalin (CS1), 19-oxo-cinobufagin (CS3), and bufarenogin (CS8). In addition, we

FIGURE 4 | The MS spectra and fragmentation pattern of taurocholic acid in positive ion mode.
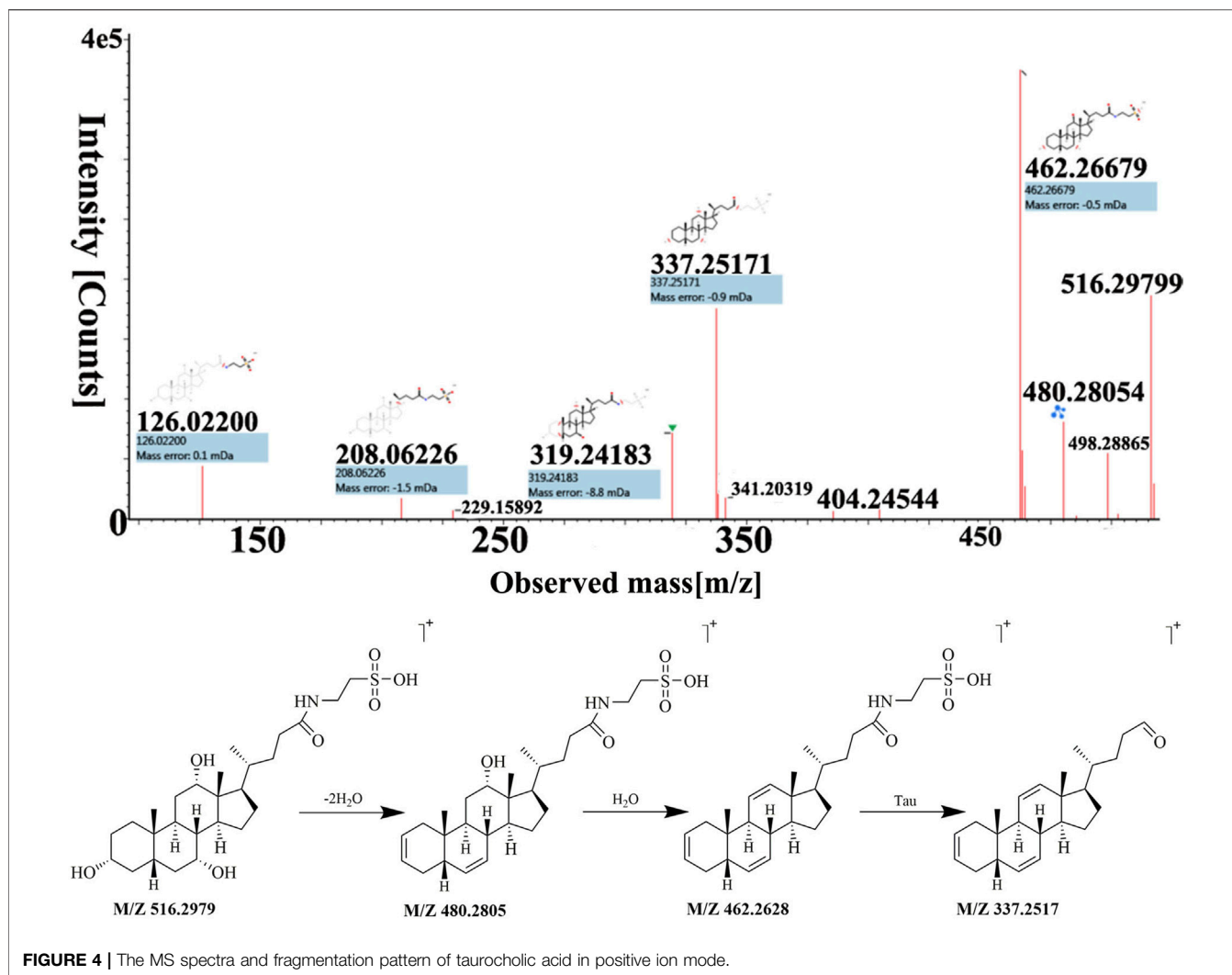
imported drug-related targets and CVDs-related targets into Cytoscape 3.7.2 software to build the protein-protein interaction (PPI) Network (**Figure 7**). The PPI network has 61 nodes and 266 edges.

3.3.3 GO and KEGG Pathway Enrichment Analysis

The Gene Ontology (GO) function enrichment analysis results of HJP for the treatment of CVDs core target genes are shown in **Figure 8A**. The biological processes mainly included positive regulation of cell migration, response to wounding, blood circulation, and positive regulation of cell migration. The main targets of cell component analysis were focal adhesion, membrane raft, receptor complex, nuclear envelope, etc. Simultaneously, molecular function terms mainly contained protein kinase activity, receptor substrate binding, cytokine receptor binding, phosphatase binding, and so on.

A total of 132 signal pathways were enriched, and 20 top-ranking pathways were screened out to analyze ($p < 0.05$). Kyoto Encyclopedia of Genes and Genomes (KEGG) pathway enrichment analysis results showed that the targets of HJP for the treatment of CVDs mainly

focused on endocrine resistance, PI3K-Akt signaling pathway, and HIF-1 signaling pathway, etc. (**Figure 8B**).

3.3.4 Component-Target-Pathway (C-T-P) Network Construction

The Merge function of Cytoscape 3.7.2 software was used to combine the effective compounds of HJP, the action targets of compounds, and the signal pathways. Afterward, visual analysis was performed to construct an overall network diagram of C-T-P (**Figure 9**). As we know, the more connections you have, the more critical it is. The results showed that 5β-hydroxybufotalin, 19-oxo-cinobufagin, and bufarenogin were the more essential ingredients. Besides, the active ingredients played a role in CVDs treatment mainly by acting on PIK3CA, MAPK1, MTOR, VEGFA, and other targets.

3.3.5 Results of Molecular Docking

We performed flexible molecular docking between the top three core active ingredients and the top two core targets. Docking binding energy below 0 indicates that two molecules can
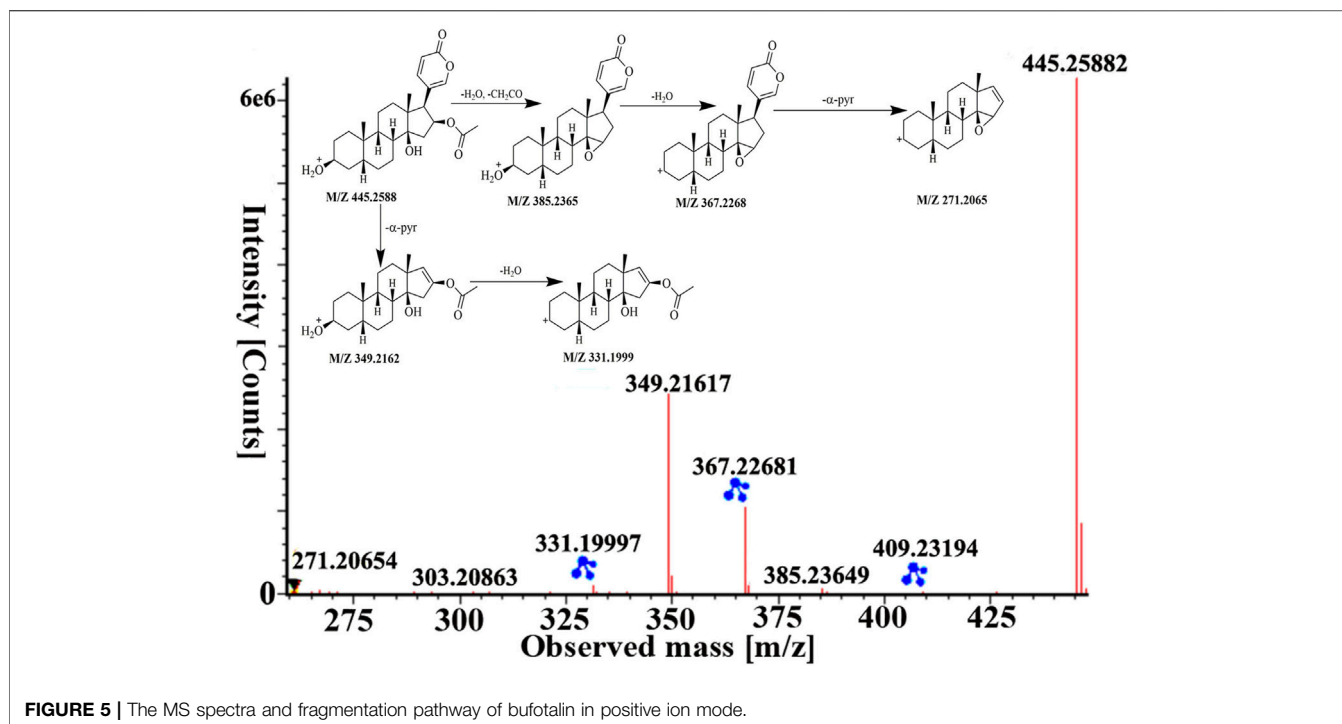
FIGURE 5 | The MS spectra and fragmentation pathway of bufotalin in positive ion mode.

TABLE 2 | Active ingredients list of HJP.

Name	Compound	Chemical formula	Source
RS1	Ginsenoside Rg$_3$	$C_{42}H_{72}O_{13}$	a
RS2	Ginsenoside Rc	$C_{53}H_{90}O_{22}$	a
RS3	Ginsenoside Rh$_1$	$C_{35}H_{60}O_9$	a
RS4	Ginsenoside Rg$_2$	$C_{42}H_{72}O_{13}$	a
RS5	Ginsenoside Rb$_1$	$C_{54}H_{92}O_{23}$	a
RS6	Ginsenoside Rf	$C_{42}H_{72}O_{14}$	a
RS7	Ginsenoside Rg$_1$	$C_{42}H_{72}O_{14}$	a
RS8	Ginsenoside Re	$C_{48}H_{82}O_{18}$	a
CS1	5β-Hydroxybufotalin	$C_{26}H_{36}O_7$	b
CS2	7β-Hydroxycholesterol	$C_{27}H_{46}O_2$	b
CS3	19-Oxo-cinobufagin	$C_{26}H_{32}O_7$	b
CS4	19-Oxo-desacetylcinobufagin	$C_{24}H_{30}O_6$	b
CS5	Bufotenidine	$C_{13}H_{18}N_2O$	b
CS6	Bufotenine	$C_{12}H_{16}N_2O$	b
CS7	Psi-bufarenogin	$C_{24}H_{32}O_6$	b
CS8	Bufarenogin	$C_{24}H_{32}O_6$	b
CS9	Resibufogenin	$C_{24}H_{32}O_4$	b
BP1	Asiatic acid	$C_{30}H_{48}O_5$	c
RGNH1	Murocholic acid	$C_{24}H_{40}O_4$	d
A1	Cholic acid	$C_{24}H_{40}O_5$	d, e
A2	Deoxycholic acid	$C_{24}H_{40}O_4$	d, e
A3	Lithocholic acid	$C_{24}H_{40}O_3$	d, e
A4	Chenodeoxycholic acid	$C_{24}H_{40}O_4$	d, e
A5	Sodium glycocholate	$C_{26}H_{42}NNaO_6$	d, e
A6	Sodium deoxycholate	$C_{24}H_{39}NaO_4$	d, e
A7	Glycocholic Acid	$C_{26}H_{43}NO_6$	d, e

[a]*Panax ginseng C. A. Meyer.*
[b]*Venenum Bufonis.*
[c]*Borneolum.*
[d]*Artificial Calculus Bovis.*
[e]*Ox Bile Powder.*

spontaneously bind, and smaller binding energy leads to a more stable conformation. Therefore, we can conclude that the core active ingredients have a good affinity for the target proteins. Furthermore, chemical components acting on multiple amino acid residues also suggest the multi-target characteristics of TCM preparation. The docking energy and its local structure are shown in **Table 3** and **Figure 10**.

4 DISCUSSION

HJP is a TCM preparation widely used to treat CVDs. However, only preliminary studies have been conducted on HJP. There were still gaps in the research on the material basis and mechanism of action of HJP in CVDs treatment. It restricted the further clinical research and market promotion of HJP. Therefore, this research has developed a comprehensive research strategy combining UPLC-Q-TOF/MS^E and network pharmacology to fill these existing gaps. Finally, this research identified and initially characterized 117 compounds, including triterpenoid saponins (32), cholic acids (13), bufadienolides 22) and others. It can be considered that the established UPLC-Q-TOF/MS^E method was more comprehensive for the detection and identification of the chemical components in HJP. The research results provided more basic information on chemical substances for the further research of HJP.

According to the constructed C-T-P network analysis, 5β-hydroxybufotalin, 19-oxo-cinobufagin, and bufarenogin were the active ingredients associated with the most targets. The results of molecular docking also verified that they have good binding
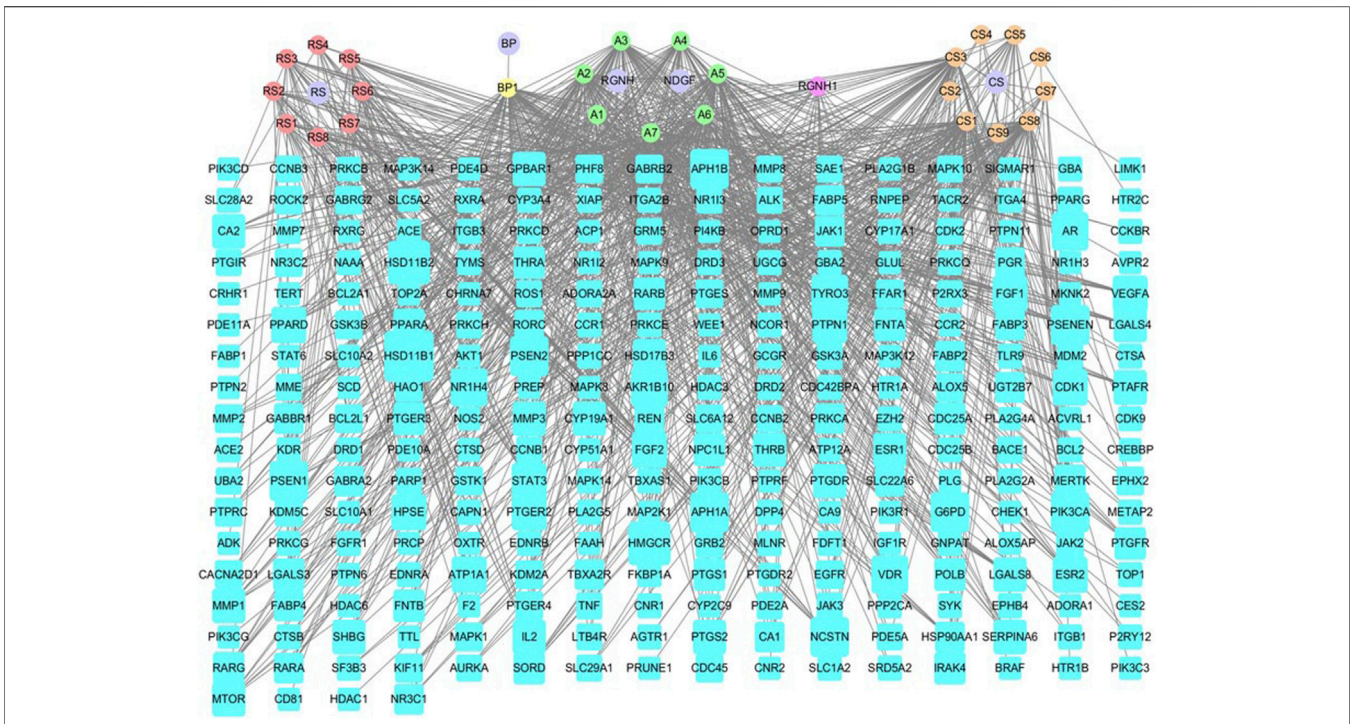
FIGURE 6 | Drug-ingredient-target network of HJP (RS: *Panax ginseng C. A. Meyer.* CS: *Venenum Bufonis.* BP: *Borneolum.* RGNH: Artificial Calculus Bovis. NDGF: Ox Bile Powder. The purple round nodes were composed of drugs surrounded by their particular ingredients. The blue rectangular node represented the gene targets.).
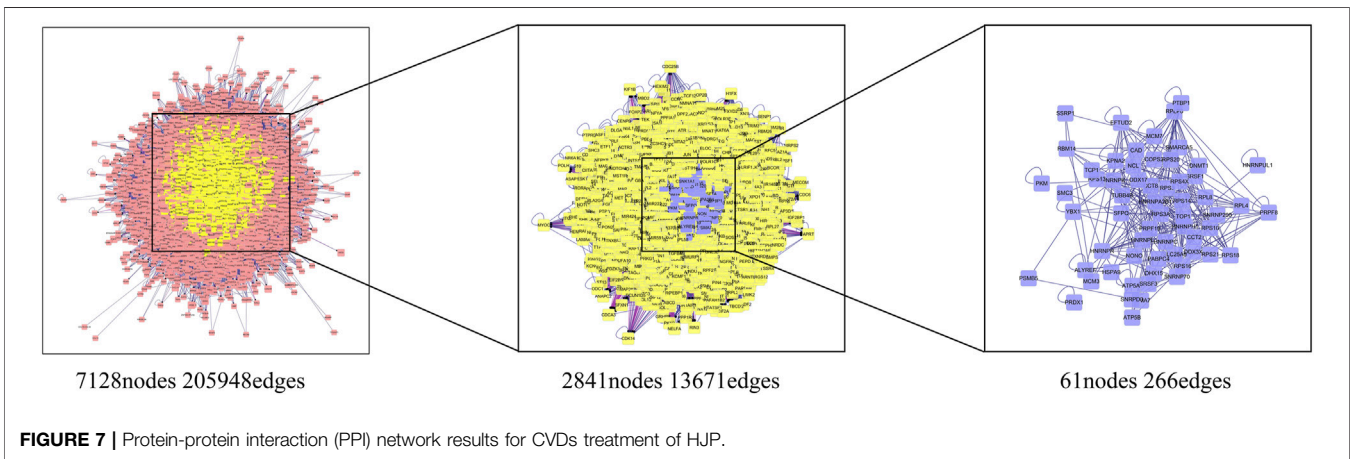

7128nodes 205948edges   2841nodes 13671edges   61nodes 266edges

FIGURE 7 | Protein-protein interaction (PPI) network results for CVDs treatment of HJP.

properties with target genes. In the current study, the results of GO and pathway enrichment analysis showed that HJP treated CVDs, which may involve the following biological processes and pathways: receptor complex, receptor substrate binding, cytokine receptor binding, endocrine resistance, PI3K-Akt signaling pathway, HIF-1 signaling pathway, and so on. According to the matching results, the CVDs-related targets of HJP were PIK3CA, MAPK1, MTOR, VEGFA, and EGFR, etc. In the following research, we will select some key targets to explore the possible mechanism of HJP in CVDs treatment.

HJP may treat CVDs by modulating the mechanism of angiogenesis. Angiogenesis is responsible for a wide variety of physio/pathological processes, including CVDs. It is strictly controlled by the balance of pro-angiogenic and anti-angiogenic factors, such as vascular endothelial growth factor (VEGF) and epidermal growth factor (EGF), etc. (Ambasta et al., 2011). Studies have shown that bufalin can target the mTOR/VEGF signaling pathway, affecting the tumor vascular microenvironment and improving the anti-angiogenic effect (Wang et al., 2018a). Gamabufotalin, an important active compound of

FIGURE 8 | GO **(A)** and KEGG pathway **(B)** enrichment analysis of results for CVD treatment of HJP.

FIGURE 9 | C-T-P network for CVDs treatment of HJP (The yellow, blue and red nodes represented the active components, gene targets, and pathways, respectively.).
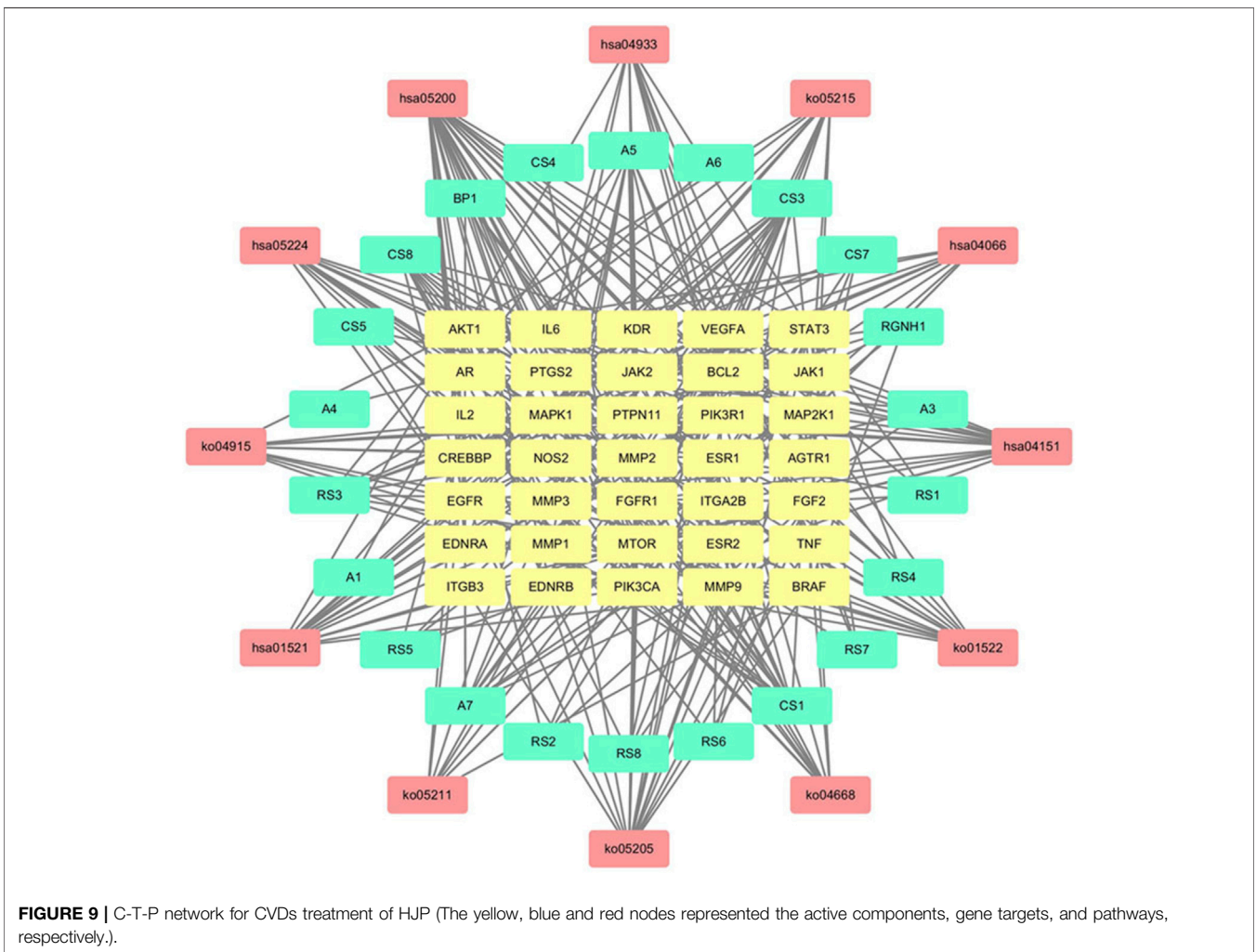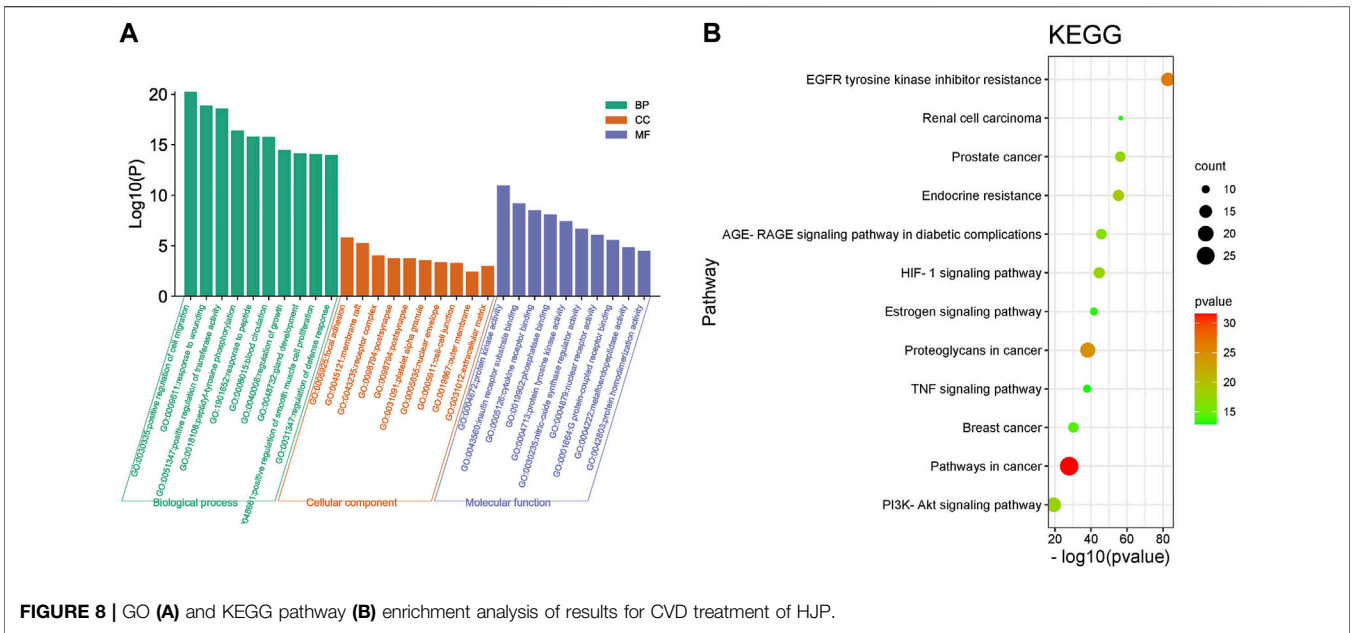
TABLE 3 | Molecular docking parameter table.

Target protein	Docking parameters	5β-Hydroxybufotalin	19-Oxo-cinobufagin	Bufarenogin
PIK3CA	binding energy/kJ·mol^{-1}	−6.01	−5.97	−5.83
	Participating amino acid residues	ASP-67, ASN-49, GLN-51	GLU-94, HIS-96, GLU-130	LYS-87, GLU-95, ASN-24
MAPK1	binding energy/kJ·mol^{-1}	−6.01	−6.68	−6.13
	Participating amino acid residues	HIS-178, ARG-172, ASN-144, GLU-334	ARG-70, ARG-172, GLU-334	GLU-334, ARG-172, PHE-331

FIGURE 10 | Molecular docking structure diagram **(A)**. PIK3CA and 5β-hydroxybufotalin **(B)**. PIK3CA and 19-oxo-cinobufagin **(C)**. PIK3CA and bufarenogin **(D)**. MAPK1 and 5β-hydroxybufotalin **(E)**. MAPK1 and 19-oxo-c.
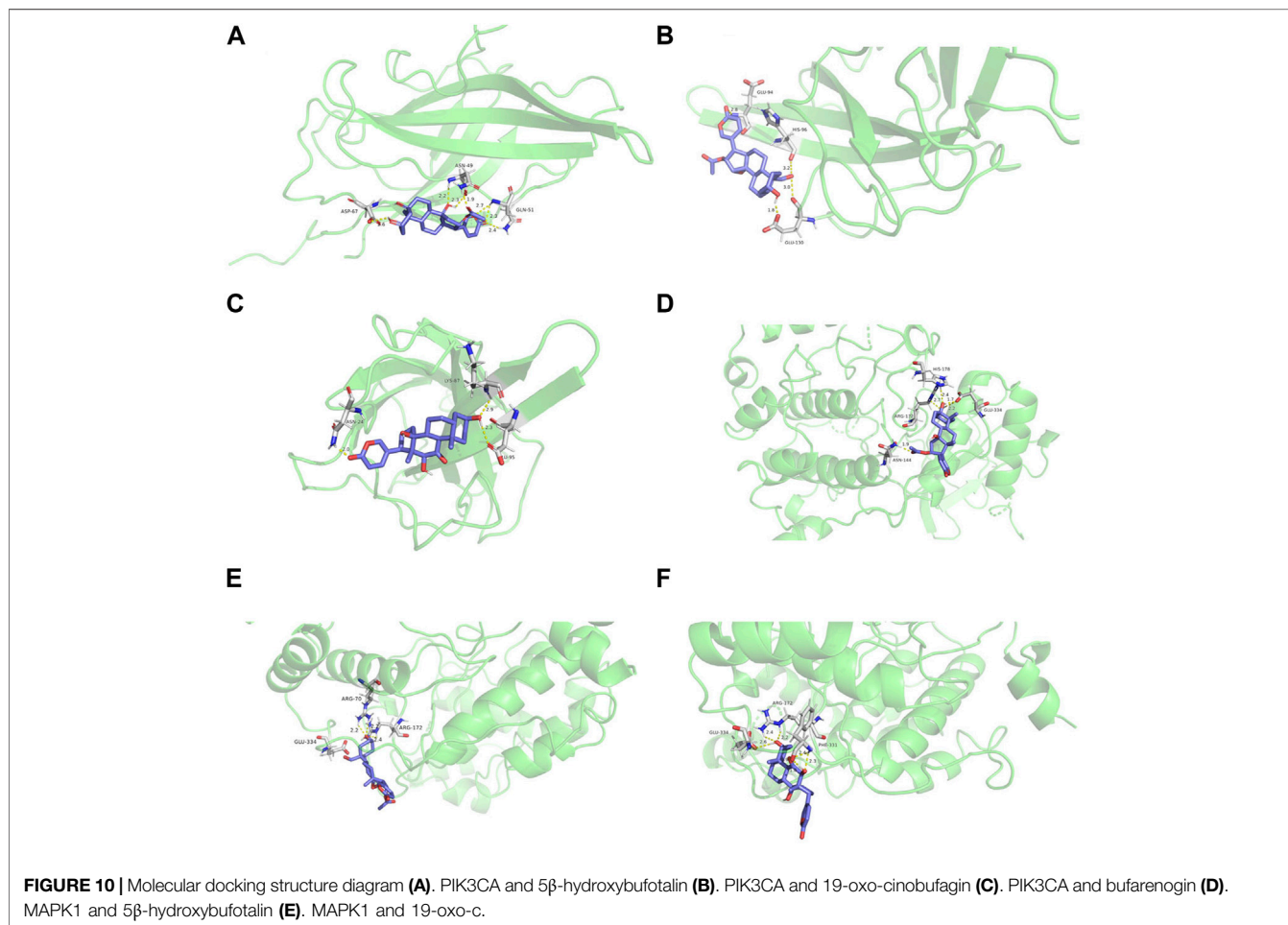
bufadienolides, was also proved as a potential anti-angiogenesis agent that targets VEGF/VEGFR-2 signaling pathways (Tang et al., 2016). Furthermore, the PIK3CA gene can increase the release of NO through the PI3K/Akt/e-NOS pathway and induce the regeneration of myocardial ischemic blood vessels (Zhang et al., 2019b). In HJP, 16 compounds, including 5β-hydroxybufotalin and bufarenogin, have been shown to have effects on PIK3CA and VEGFA by the C-T-P network.

On the other hand, HJP can regulate inflammation and oxidative stress targets to treat CVDs. The most promising intervention direction for atherosclerosis is lipid metabolism and inflammation. And inflammatory factors are involved in the occurrence and development of CVDs. For instance, MAPK1 is involved in various physiological and pathological processes, such as the body's adaptive response to external environmental stress and inflammation. It is the common target of many anti-inflammatory drugs and can promote the production of IL-β and TNF-α, pro-inflammatory cytokines that can activate enzymes related to inflammation. In addition, studies have found that Ginsenoside Re is a powerful antioxidant protecting cardiomyocytes from oxidation by scavenging free radicals (Wang et al., 2018b). And Taurodeoxycholic acid can regulate the MAPK and NF-KB pathways and promote the anti-inflammatory cytokine IL-10 (Ko et al., 2017). Glycocholic acid and glycosyllithocholic acid can reduce the synthesis and release of nitric oxide, inhibit the production of leukotriene B$_4$ and prostaglandin E$_2$, and produce anti-inflammatory effects (Li, 2006). These selected active ingredients in HJP played an important role in treating CVDs and provide a reference for more in-depth material basic research.

5 CONCLUSION

This study used integrated research on chemical profiling to explore the chemical constituents and action mechanism of HJP by UPLC-Q-TOF/MS^E and network pharmacology. Finally, on the basis of the research on the chemical composition of HJP, we initially revealed that HJP might exert therapeutic effects on CVDs by regulating the mechanism of angiogenesis, inflammation, and oxidative stress targets.

On the one hand, this paper provides a certain basis and reference for the further study of the pharmacodynamic material basis and *in vivo* mechanism of HJP. On the other hand, the integrated methods and results it established also provide some reference for other basic research on TCM. However, we contrast the network pharmacology research content in this paper with the latest Network pharmacology evaluation method guidance (Li et al., 2021). It was found that the verification experiment used a combination of computer-aided and literature data. Although the overall experiment satisfies the standardization and rationality, the reliability has certain limitations. Therefore, in the future, we will use the Network pharmacology evaluation method guidance as a guide to experimentally verify the results to further increase their reliability.

DATA AVAILABILITY STATEMENT

The datasets presented in this study can be found in online repositories. The names of the repository/repositories and accession number(s) can be found in the article/**Supplementary Material**.

AUTHOR CONTRIBUTIONS

YLZ and YJZ have made substantial contributions to the conception or design of the work; or the acquisition, analysis, or interpretation of data for the work. CP, HW, and DW have drafted the work or revised it critically for important intellectual content. ST, WL, JZ, YZ, ZX, and JX have approved the final version to be published.

FUNDING

SUPPLEMENTARY MATERIAL

The Supplementary Material for this article can be found online at: https://www.frontiersin.org/articles/10.3389/fmolb.2022.818285/full#supplementary-material

REFERENCES

Ambasta, R. K., Sharma, A., and Kumar, P. (2011). Nanoparticle Mediated Targeting of VEGFR and Cancer Stem Cells for Cancer Therapy. *Vasc. Cel* 3, 26. doi:10.1186/2045-824x-3-26

Chen, X., Yao, F., Song, J., Fu, B., Sun, G., Song, X., et al. (2020). Protective Effects of Phenolic Acid Extract from Ginseng on Vascular Endothelial Cell Injury Induced by Palmitate via Activation of PI3K/Akt/eNOS Pathway. *J. Food Sci.* 85 (3), 576–581. doi:10.1111/1750-3841.15071

Damiani, I., Corsini, A., and Bellosta, S. (2020). Potential Statin Drug Interactions in Elderly Patients: a Review. *Expert Opin. Drug Metab. Toxicol.* 16 (12), 1133–1145. doi:10.1080/17425255.2020.1822324

Deprince, A., Haas, J. T., and Staels, B. (2020). Dysregulated Lipid Metabolism Links NAFLD to Cardiovascular Disease. *Mol. Metab.* 42, 101092. doi:10.1016/j.molmet.2020.101092

Floreani, A. (2020). Experimental Pharmacological Agents for the Treatment of Primary Biliary Cholangitis. *Jep* Vol. 12, 643–652. doi:10.2147/jep.s267375

Fu, J., Wu, H., Wu, H., Deng, R., and Li, F. (2019). Chemical and Metabolic Analysis of Achyranthes Bidentate Saponins with Intestinal Microflora-Mediated Biotransformation by Ultra-performance Liquid Chromatography-Quadrupole Time-Of-Flight Mass Spectrometry Coupled with Metabolism Platform. *J. Pharm. Biomed. Anal.* 170, 305–320. doi:10.1016/j.jpba.2019.03.041

Halaris, A. (2017). Inflammation-Associated Co-morbidity between Depression and Cardiovascular Disease. *Curr. Top. Behav. Neurosci.* 31, 45–70. doi:10.1007/7854_2016_28

Hu, S., Wu, Y., Zhao, B., Hu, H., Zhu, B., Sun, Z., et al. (2018). Panax Notoginseng Saponins Protect Cerebral Microvascular Endothelial Cells against Oxygen-Glucose Deprivation/Reperfusion-Induced Barrier Dysfunction via Activation of PI3K/Akt/Nrf2 Antioxidant Signaling Pathway. *Molecules* 23 (11), 2781. doi:10.3390/molecules23112781

Ko, W. K., Lee, S. H., Kim, S. J., Jo, M. J., Kumar, H., Han, I. B., et al. (2017). Anti-inflammatory Effects of Ursodeoxycholic Acid by Lipopolysaccharide-Stimulated Inflammatory Responses in RAW 264.7 Macrophages. *PLOS One* 12 (6), e0180673. doi:10.1371/journal.pone.0180673

Li, H. F. (2006). *Study on Anti-inflammatory Mechanism of Glycocholic Acid [D].* Inner Mongolia: Inner Mongolia Agricultural University.

Li, S., Chen, Y. T., and Ding, Q. Y. (2021). Network Pharmacology Evaluation Method guidance-Draft. *World J. Tradit Chin. Med.* 7 (1), 146–154. doi:10.4103/wjtcm.wjtcm_11_21

Li, S., and Zhang, B. (2013). Traditional Chinese Medicine Network Pharmacology: Theory, Methodology and Application. *Chin. J. Nat. Medicines* 11 (2), 110–120. doi:10.1016/s1875-5364(13)60037-0

Luo, J., Ren, Y., Gu, H., Wu, Y., and Wang, Y. (2013). dTGS: Method for Effective Components Identification from Traditional Chinese Medicine Formula and Mechanism Analysis. *Evid. Based Complement. Alternat Med.* 2013, 840427. doi:10.1155/2013/840427

Tang, N., Shi, L., Yu, Z., Dong, P., Wang, C., Huo, X., et al. (2016). Gamabufotalin, a Major Derivative of Bufadienolide, Inhibits VEGF-Induced Angiogenesis by Suppressing VEGFR-2 Signaling Pathway. *Oncotarget* 7 (3), 3533–3547. doi:10.18632/oncotarget.6514

Taskinen, M.-R., and Borén, J. (2015). New Insights into the Pathophysiology of Dyslipidemia in Type 2 Diabetes. *Atherosclerosis* 239 (2), 483–495. doi:10.1016/j.atherosclerosis.2015.01.039

Wang, H., Zhang, C., Chi, H., and Meng, Z. (2018). Synergistic Anti-hepatoma Effect of Bufalin Combined with Sorafenib via Mediating the Tumor Vascular Microenvironment by Targeting mTOR/VEGF Signaling. *Int. J. Oncol.* 52 (6), 2051–2060. doi:10.3892/ijo.2018.4351

Wang, K., Chen, Q., Shao, Y., Yin, S., Liu, C., Liu, Y., et al. (2021). Anticancer Activities of TCM and Their Active Components against Tumor Metastasis. *Biomed. Pharmacother.* 133, 111044. doi:10.1016/j.biopha.2020.111044

Wang, Q. W., Yu, X. F., Xu, H. L., Jiang, Y. C., Zhao, X. Z., and Sui, D. Y. (2018). Ginsenoside Re Attenuates Isoproterenol-Induced Myocardial Injury in Rats. *Evid. Based Complement. Alternat Med.* 2018, 8637134. doi:10.1155/2018/8637134

Wang, X., Wang, Z.-Y., Zheng, J.-H., and Li, S. (2021). TCM Network Pharmacology: A New Trend towards Combining Computational, Experimental and Clinical Approaches. *Chin. J. Nat. Medicines* 19 (1), 1–11. doi:10.1016/s1875-5364(21)60001-8

Wansapura, A. N., Lasko, V., Xie, Z., Fedorova, O. V., Bagrov, A. Y., Lingrel, J. B., et al. (2009). Marinobufagenin Enhances Cardiac Contractility in Mice with Ouabain-Sensitive α1Na+-K+-ATPase. *Am. J. Physiology-Heart Circulatory Physiol.* 296 (6), H1833–H1839. doi:10.1152/ajpheart.00285.2009

Wei, M., Li, H., Li, Q., Qiao, Y., Ma, Q., Xie, R., et al. (2020). Based on Network Pharmacology to Explore the Molecular Targets and Mechanisms of Gegen Qinlian Decoction for the Treatment of Ulcerative Colitis. *Biomed. Res. Int.* 2020, 5217405. doi:10.1155/2020/5217405

Xie, S., Spelmink, L., Codemo, M., Subramanian, K., Pütsep, K., Henriques-Normark, B., et al. (2016). Cinobufagin Modulates Human Innate Immune Responses and Triggers Antibacterial Activity. *PLoS One* 11 (8), e0160734. doi:10.1371/journal.pone.0160734

Xu, L., Liu, Y., Wu, H., Wu, H., Liu, X., and Zhou, A. (2020). Rapid Identification of Chemical Profile in Gandou Decoction by UPLC-Q-TOF-MSE Coupled with Novel Informatics UNIFI Platform. *J. Pharm. Anal.* 10 (1), 35–48. doi:10.1016/j.jpha.2019.05.003

Xu, X., Wang, M., Li, J.-z., Wei, S.-D., Wu, H., Lai, X., et al. (2018). Tauroursodeoxycholic Acid Alleviates Hepatic Ischemia Reperfusion Injury by Suppressing the Function of Kupffer Cells in Mice. *Biomed. Pharmacother.* 106, 1271–1281. doi:10.1016/j.biopha.2018.06.046

Zhang, J.-j., Zhou, X.-h., Zhou, Y., Wang, Y.-g., Qian, B.-z., He, A.-n., et al. (2019). Bufalin Suppresses the Migration and Invasion of Prostate Cancer Cells through HOTAIR, the Sponge of miR-520b. *Acta Pharmacol. Sin* 40 (9), 1228–1236. doi:10.1038/s41401-019-0234-8

Zhang, X., Huang, L. F., Hua, L., Feng, H. K., and Shen, B. (2019). Resveratrol Protects Myocardial Apoptosis Induced by Ischemia-Reperfusion in Rats with Acute Myocardial Infarction via Blocking P13K/Akt/e-NOS Pathway. *Eur. Rev. Med. Pharmacol. Sci.* 23 (4), 1789–1796. doi:10.26355/eurrev_201902_17142

Zhou, W. L., Zhong, Q. S., and Peng, C. (2020). Preliminary Study on the Effect of Huatuo Jiuxin Pills on Myocardial Ischemia and Blood Circulation and Stasis Removal [J]. *Cent. south Pharm.* 18 (03), 402–406.